SUPPLEMENTARY DATA

Comprehensive spectroscopic analysis of energy inversion of the lowest singlet and triplet excited states in the heptazine $HzTFEX_2$

Carolina Francener[a], Hector Miranda-Salinas[a], Christopher J. Riggs[a], Naoya Aizawa[b,c] and Andrew Monkman[a*]

[a] OEM-Research Group, Dept of Physics, University of Durham, South Road, Durham, DH1 3LE, UK.

[b] Institute for Chemical Reaction Design and Discovery (WPI-ICReDD), Hokkaido University, Sapporo, Hokkaido 001-0021, Japan.

[c] Division of Applied Chemistry, Graduate School of Engineering, the University of Osaka, Suita, Osaka, 565-0871, Japan.

*Email: a.p.monkman@durham.ac.uk

1. Initial characterization in solution

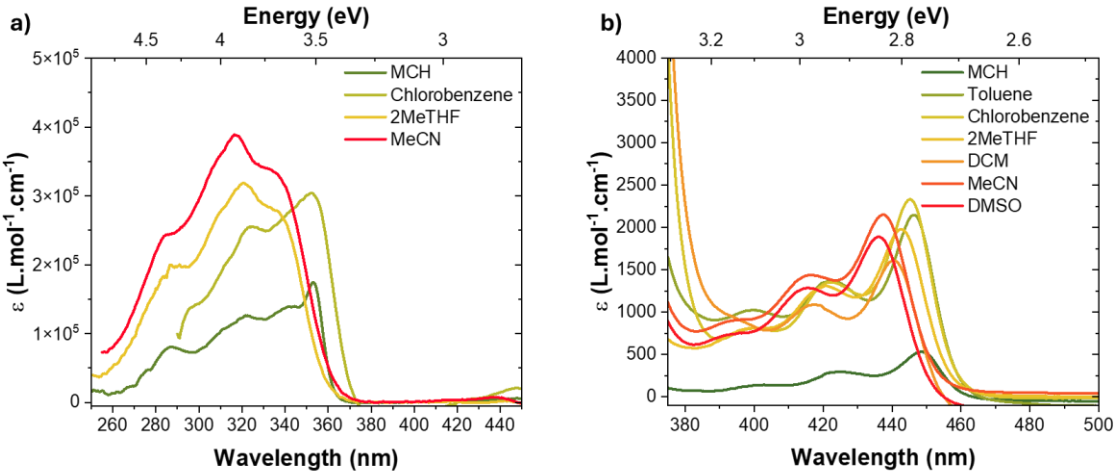

Figure S1. Absorption in solution. Absorption of $HzTFEX_2$ depicting **(a)** high energy bands (0.2 μM) and **(b)** low energy bands (20 μM) in a range of solvents. A 5 cm path cuvette was used for measuring the 20 μM solutions.

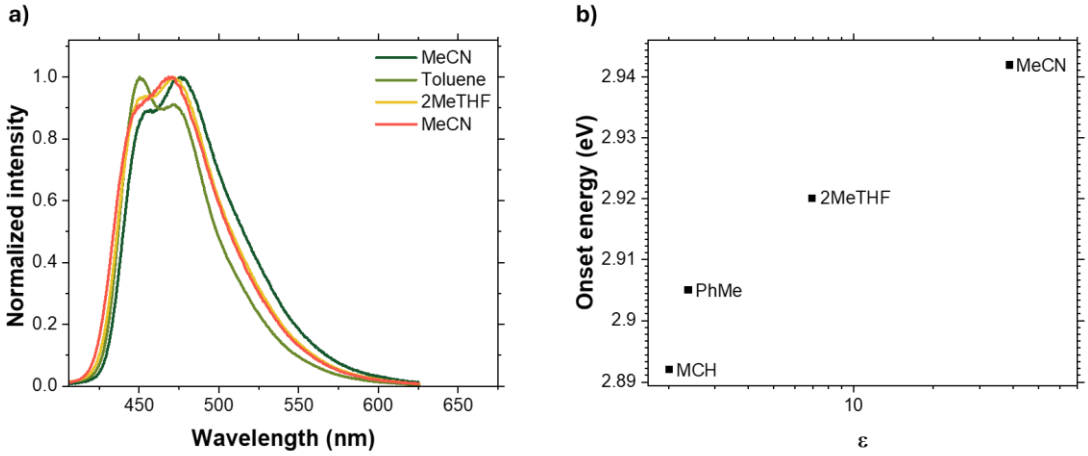

Figure S2. Solvent dependency of the photoluminescence. a) PL of $HzTFEX_2$ in a range of solvents at 2μM measured at room temperature. λ_{ex} = 355 nm. b) PL onset energy against solvent dielectric constat (ε).

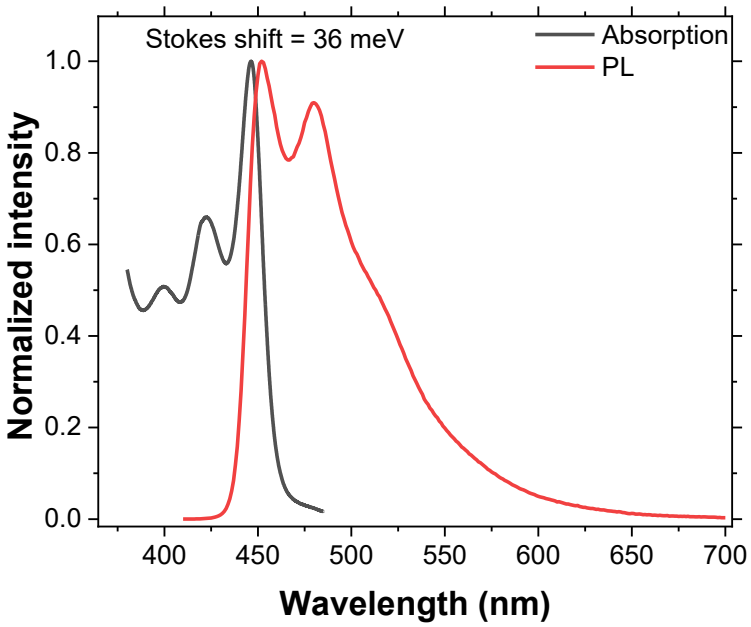

Figure S3. Stokes shift of S_1. Absorption and PL of $HzTFEX_2$ in 20 μM toluene solution. λ_{ex} = 355 nm.

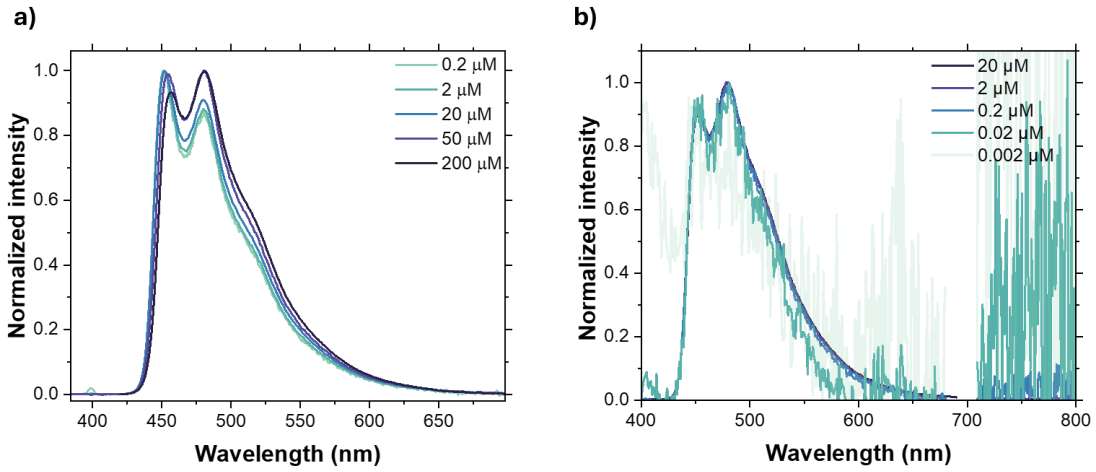

Figure S4. Concentration dependency of the photoluminescence. PL of $HzTFEX_2$ in (a) toluene and (b) 2-MeTHF in a range of concentrations. λ_{ex} = 355 nm.

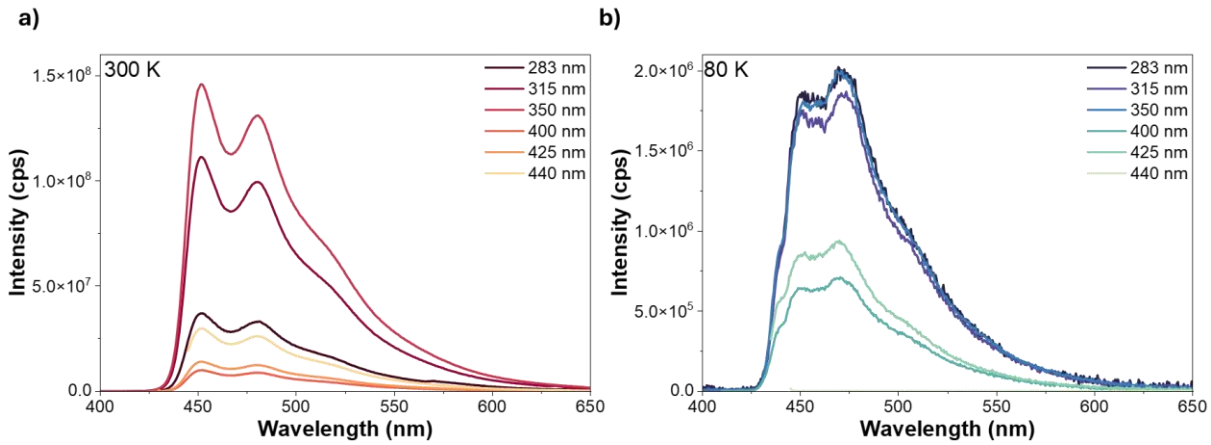

Fig S5. Dimer concentration dependency on temperature. PL of $HzTFEX_2$ in toluene 20 µM solution monitored at (a) room temperature and (b) 80 K. λ_{ex} = 355 nm.

1.1. Photoluminescence in the presence of a triplet quencher

To probe the singlet or triplet character of the PL at room temperature, the triplet quencher cyclooctatetraene (COT) was added to a 20 µM solution in excess (10% wt/wt) (Figure S6). It was found that the presence of COT doesn't affect the spectral shape of the PL of $HzTFEX_2$, nor does it have an impact on the lifetime of the emission. Therefore, emission of $HzTFEX_2$ at room temperature is determined to arise from the singlet manifold.

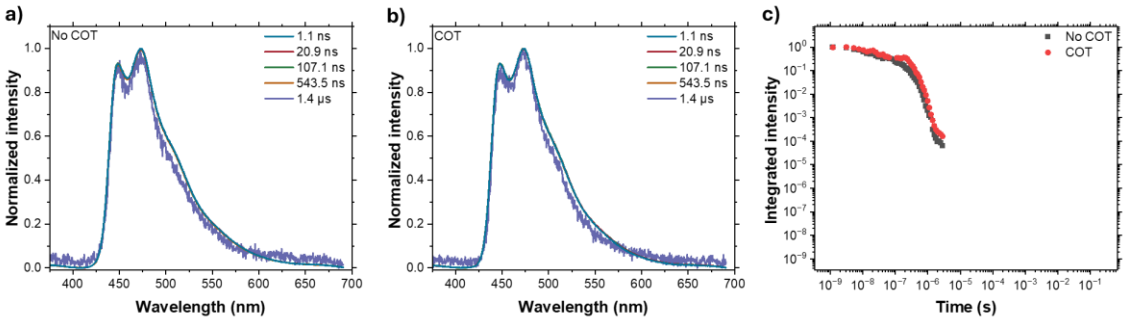

Figure S6. Impact of a triplet quencher on the time-resolved photoluminescence. (a) TRPL of $HzTFEX_2$ in toluene 20 µM recorded at room temperature. (b) PL of $HzTFEX_2$ in toluene 20 µM doped with COT (10% wt/wt) recorded at room temperature. (c) Decay curves of $HzTFEX_2$ with and without COT. λ_{ex} = 355 nm.

1.2. Photoluminescence quantum yield (PLQY)

Air saturated 2 µM solution of $HzTFEX_2$ in 2-MeTHF yielded a quantum efficiency of 33% (λ_{ex} = 345 nm) and 42% (λ_{ex} = 325 nm). The excitation energy dependency of the PLQY is a product of the overlap of the monomeric and dimeric absorption bands, resulting in different state populations across varying pump energies. PLQY (λ_{ex} = 345 nm) increased to 41% when solution was degassed by argon bubbling (a 24% improvement) due to diminished singlet quenching by O_2, which is significant in this system since dimer exhibits τ_{PF} > 100 ns and monomer τ_{PF} > 10 ns. Solutions cooled to 80 K yielded PLQY above 100 % (124% (λ_{ex} = 325 nm) and 168% (λ_{ex} = 345 nm)). However, this is understood by the dynamics between monomeric and dimeric species in solution. PL intensity of a 2 µM 2-MeTHF solution degassed by argon bubbling was found to decrease by 17% after the solution was allowed to stand at room temperature (20 – 15 C) for 5 min due to dimerization (Figure S7). Therefore, since dimer species have a lower quantum efficiency than the monomer and the solution has [monomer]:[dimer] ratio which is time dependent, the PLQY is, consequently, also time dependent. This leads to possible over / underestimation of quantum efficiency values, dependent on the dimer content of the solutions used as reference. However, it is possible to affirm that PLQY reaches values near 100% when dimers are mostly quenched, by considering the pronounced increase in PL intensity and spectral shape between 2-MeTHF solution at room temperature and 80 K. Finally, despite the dilute concentration of 2 µM, the molecules dimerize over time when solution isn't under heating or agitation, further indicating that $HzTFEX_2$ is highly prone to aggregation.

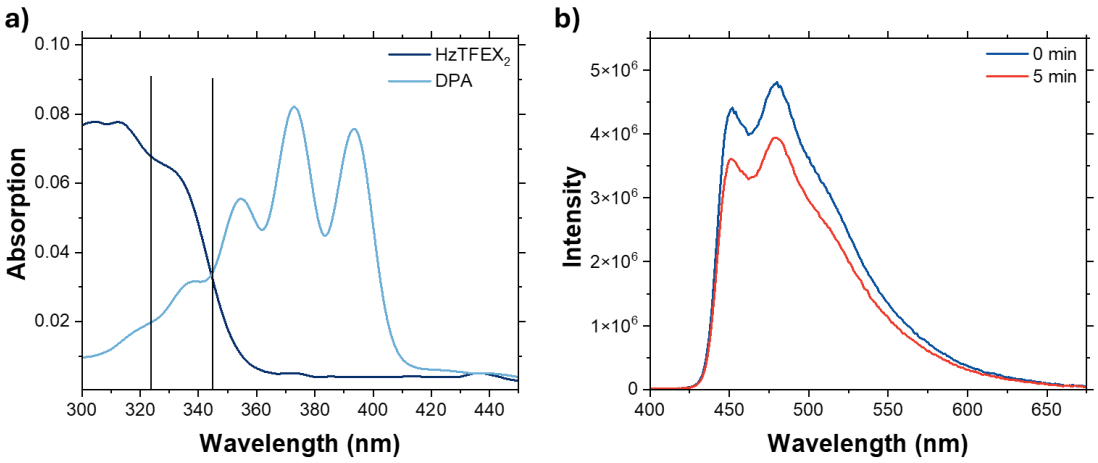

Figure S7. Determination of relative quantum efficiency. (a) Absorption spectra of $HzTFEX_2$ and DPA. Wavelengths employed for calculating the PLQY are indicated. (a) PL of degassed 2 μM 2-MeTHF solution at 0 minutes and at 5 minutes after left in static condition at room temperature. λ_{ex} = 355 nm.

2. Crystal data

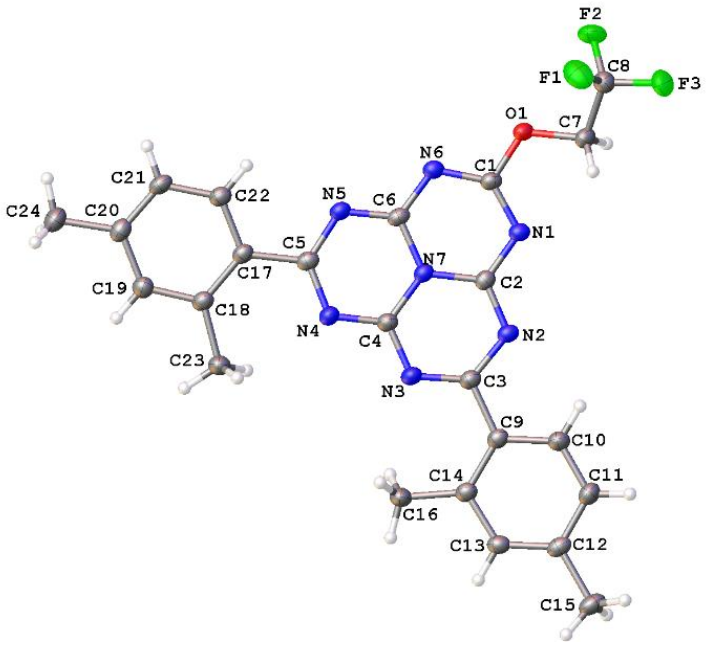

Figure S8. Molecular structure of $HzTFEX_2$. Crystal structure of $HzTFEX_2$, with the anisotropic displacement parameters depicted at the 50% probability level and disorder hidden for clarity.

Table S1. Crystal data and structure refinement for $HzTFEX_2$.

CCDC number	2551605
Empirical formula	$C_{24}H_{20}F_3N_7O$
Formula weight	479.47
Temperature/K	296.15
Crystal system	triclinic
Space group	P-1
a/Å	8.1912(5)
b/Å	11.5948(7)
c/Å	13.1174(8)
α/°	109.544(2)
β/°	93.958(2)
γ/°	109.127(2)
Volume/$Å^3$	1086.68(12)
Z	2
$\rho_{calc}g/cm^3$	1.465
μ/mm^{-1}	0.113
F(000)	496.0
Crystal size/mm^3	0.432 × 0.129 × 0.06
Radiation	MoKα (λ = 0.71073)
2Θ range for data collection/°	4.018 to 53.464
Index ranges	$-10 \leq h \leq 10$, $-14 \leq k \leq 14$, $-16 \leq l \leq 16$
Reflections collected	28844
Independent reflections	4626 [R_{int} = 0.0475, R_{sigma} = 0.0343]
Data/restraints/parameters	4626/0/320
Goodness-of-fit on F^2	1.054
Final R indexes [I>=2σ (I)]	R_1 = 0.0510, wR_2 = 0.1210

Final R indexes [all data]	R_1 = 0.0671, wR_2 = 0.1300
Largest diff. peak/hole / e Å^{-3}	0.29/-0.28

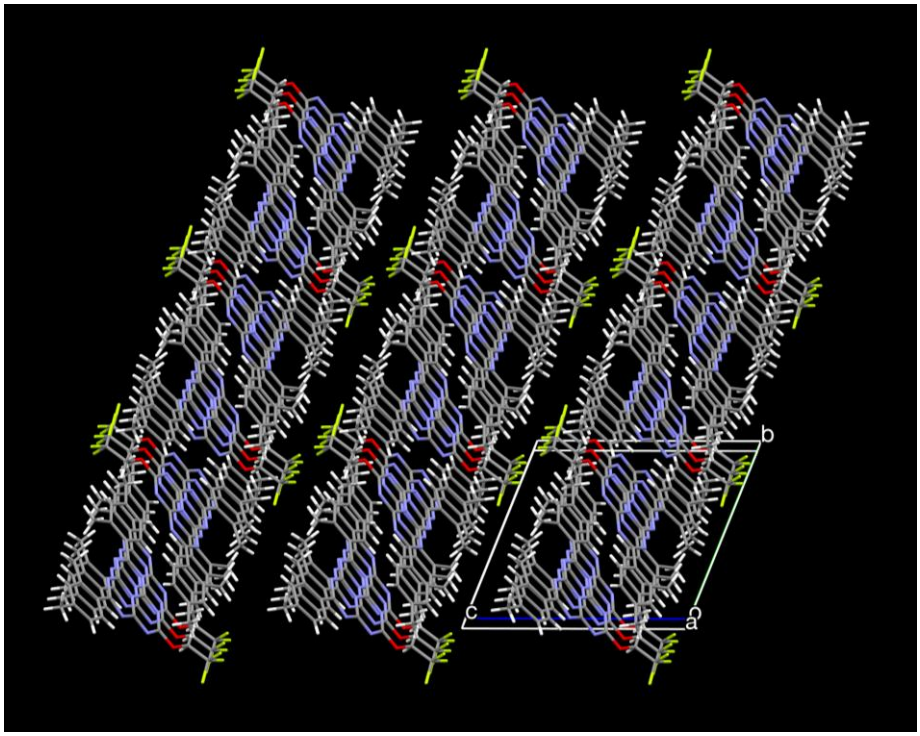

Fig S9. Molecular packing in the single crystal. Crystal structure of $HzTFEX_2$ depicting the J-like packing between the aromatic cores and the 2D layer structure.

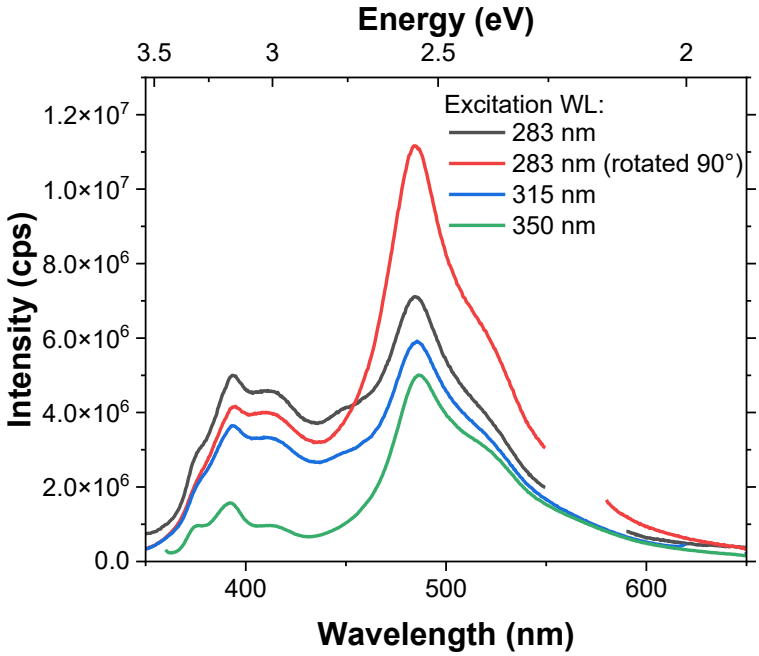

Figure S10. Unnormalized single crystal photoluminescence. PL of a single crystal of $HzTFEX_2$. Excitation wavelengths are indicated.

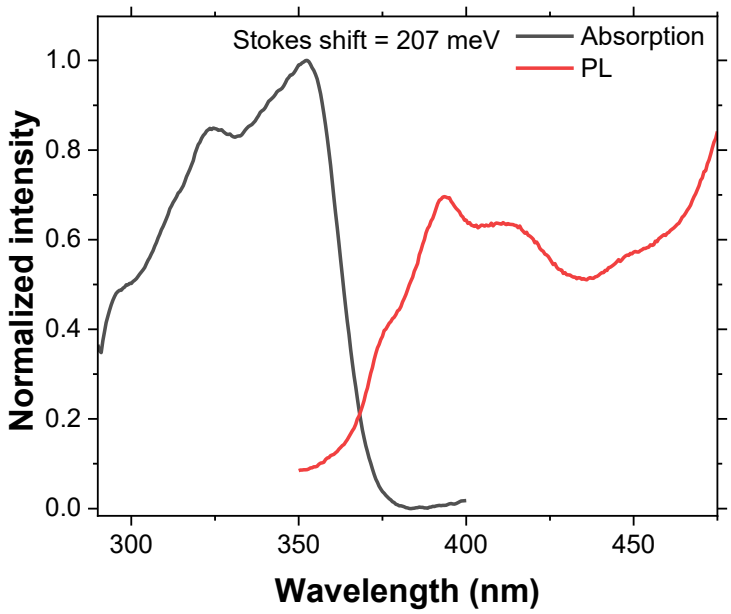

Figure 11. Stokes shift of S_2. Absorption of $HzTFEX_2$ in chlorobenzene 0.2 µM and PL of a single crystal. λ_{ex} = 283 nm.

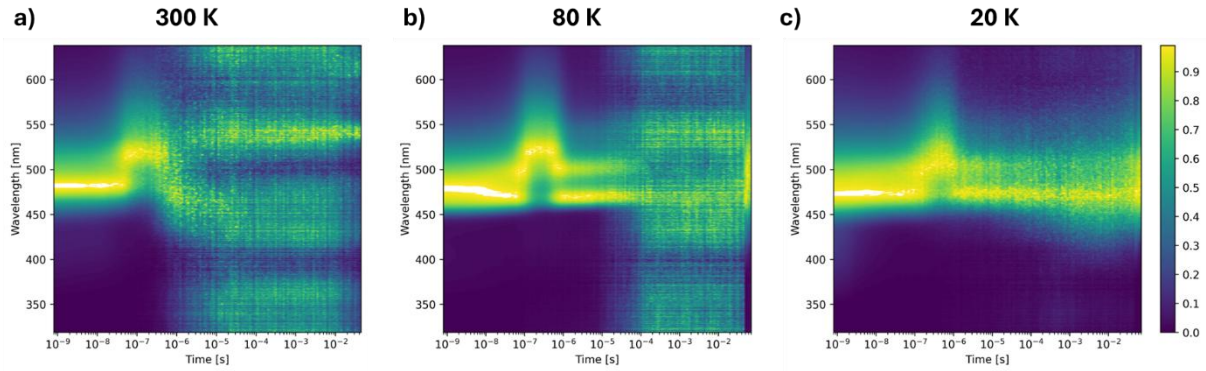

Figure S12. Temperature dependent time-resolved photoluminescence of single crystal. Contour plots of the decay of a single crystal of $HzTFEX_2$ at (a) 300 K, (b) 80 K and (c) 20 K. λ_{ex} = 355 nm.

3. Powder data

Steady-state and time-resolved emission from powder samples were measured at room temperature (Fig S13 and 14). Again, as in the crystals, a characteristic weakly structured emission band centred at 485 nm dominates, with a weak intensity, red edge feature, whose intensity increases subtly with increasing excitation wavelength. $S_0 \leftarrow S_2$ transition emission component is not observed, likely due to self-absorption. Time-resolved emission from powder samples at RT (Fig S13b) shows dominance of the 485 nm transition in the first 20 ns, with the steady emergence of the 520 nm emission at longer times. At 80 K, (Fig S13c), once the dimer states have decayed, we are left with the well-structured delayed emission band (delay time DT = 2.0 μs), the peak of the 0-0 mode being at 465 nm, matching that observed for the $S_0 \leftarrow S_1$ transition in the solution spectra (Fig 1d). Since DF from $S_0 \leftarrow S_1$ was only observed at 80 K, this eliminates the possibly of it arising from a thermally activated process and points to a TTA mechanism, facilitated by longer triplet migration distances at low temperature. Decay of prompt fluorescence is composed of two components. Shorter lived component is not affected by temperature (τ_{RT} = 9.4 ns and τ_{80K} = 10.8 ns). Conversely, longer lived emission undergoes a 4-fold increase (τ_{RT} = 57.5 ns and τ_{80K} = 212.6 ns) (Fig S15 and 16). A long-lived emission, well into the millisecond times is observed, which we assume to be weak phosphorescence (Fig S17). However, this very weak long-lived emission has peaks at 460 nm peak, 39 meV above the highly structured 465 nm $S_0 \leftarrow S_1$, which could indicate inversion.

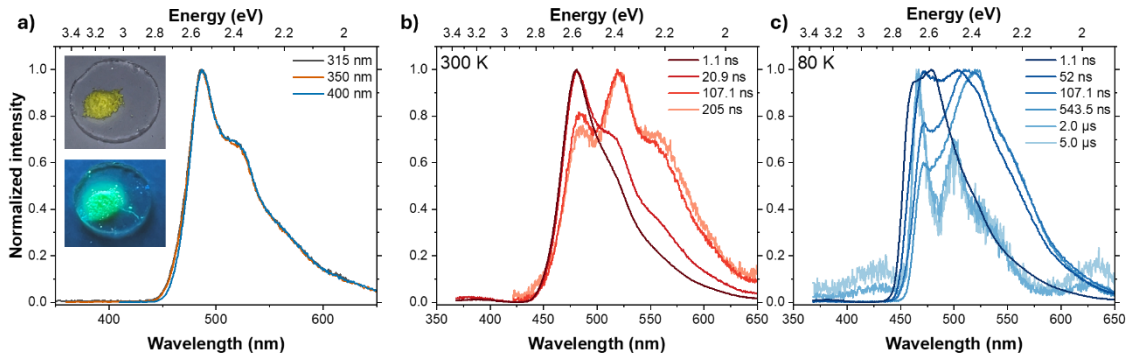

Figure S13. Photoluminescence in powder state. (a) PL of $HzTFEX_2$ powder monitored at RT. Inset shows powder under ambient light (top) and 365 nm excitation (bottom). Excitation wavelengths are indicated. TRPL of $HzTFEX_2$ powder monitored at **(b)** RT and **(c)** 80 K. λ_{ex} = 355 nm.

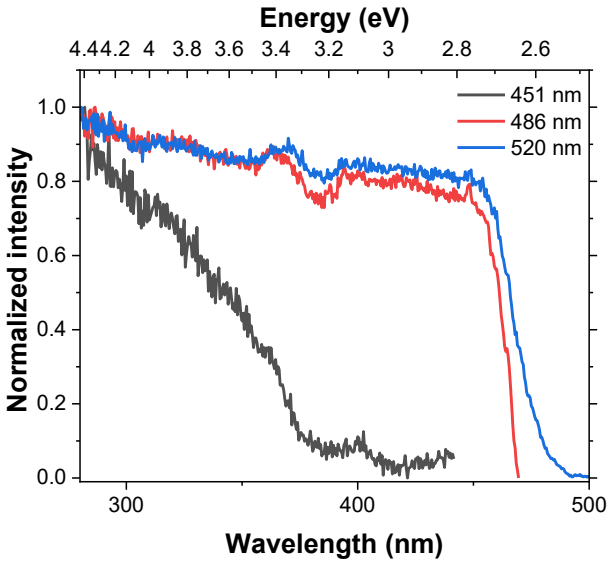

Figure S14. Excitation in powder. Excitation profile of $HzTFEX_2$ in powder state monitored at RT. Monitored wavelengths are indicated.

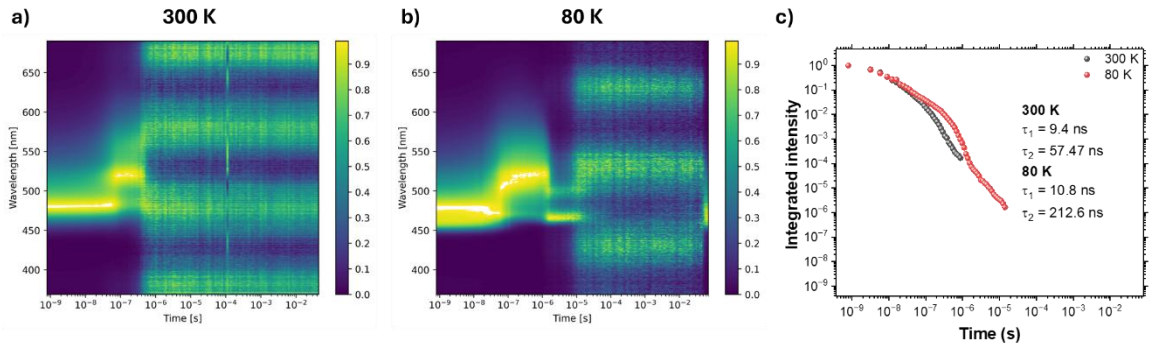

Fig S15. Time-resolved photoluminescence of powder. Contour plot of the decay of $HzTFEX_2$ powder monitored at (a) RT and (b) 80 K. (c) Decay curve of $HzTFEX_2$ in powder state at RT and 80 K. λ_{ex} = 355 nm.

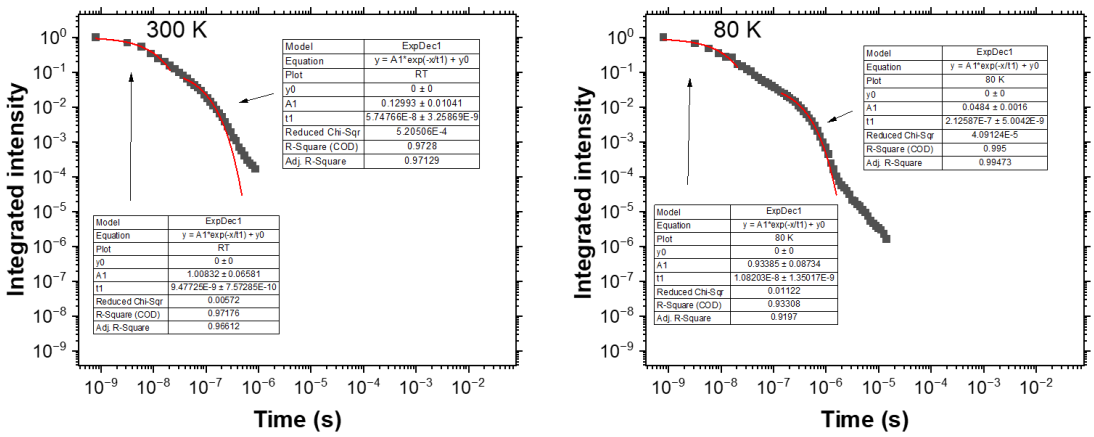

Fig S16. Fluorescence lifetimes of powder. Decay curves of $HzTFEX_2$ in powder state at RT and 80 K. The data were fitted to a monoexponential equation. λ_{ex} = 355 nm.

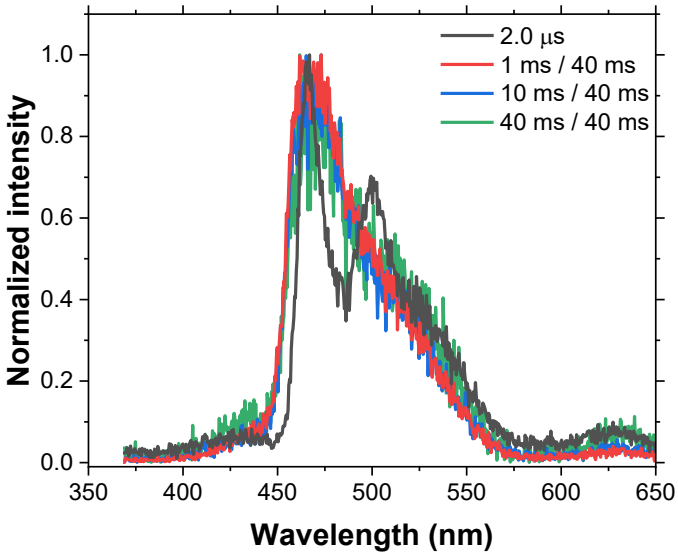

Fig S17. Long-lived emission of powder. PL at DT = 2.0 µs and time-resolved curves with millisecond delay time of $HzTFEX_2$ in powder form at 80 K. Legends indicated DT / IT used for spectra acquisition. λ_{ex} = 355 nm.

4. Guest-host films

4.1. Polystyrene (PS)

Polystyrene was used as an analogue to toluene. Emission at room temperature of a film containing 0.01% wt/wt $HzTFEX_2$ shows a mixture of monomer emission at 450 nm and 480 nm dimer emission (Fig S18). The relative dimer contribution increases when exciting at 355 nm, as compared to exciting directly into the $S_0 \rightarrow S_2$ transition. As the temperature decreases, we observe a small monotonic blue shift of the 450 nm band to 445 nm (80 K). The intensity initially drops, over the first 40 K, then recovers down to 80 K. The on-set

of emission does not change at all with temperature and no new blue edge feature appears. We observe a gradual increase in relative dimer contribution (Fig S19) which we believe is the cause of both the small monomer peak blue shift and recovery of intensity. With 355 nm excitation, the dimer emission grows more strongly indicative of direct dimer excitation as well as energy transfer excitation from the monomer excited states.

Time-resolved PL at room temperature (Fig S20a) shows a small $S_0 \leftarrow S_2$ signal (DT = 2.0 ns) and the combined decay of the monomer and dimer emissions. At 20 K, similar behaviour is observed, with increased contribution from aggregated species (Fig S20b). We observe both monomer and dimer weak emission into the microsecond which indicates a weak DF component. At 0.1% wt/wt doping concentration measured at 20 K (Fig S21a), monomer contribution to the fluorescence diminishes and emission, 470 nm peak, indicates mainly dimerized species. Long-lived emission in the millisecond (Fig S21b) is observed, still with a peak at 470 nm and a small blue foot. The weak signal, peak at 420-425 nm, could be monomer phosphorescence. Excitation fluence measurements could only be made over a long integration time, effectively covering the whole delayed emission from 300 µs (Fig. S22). In the spectral region 440 nm to 600 nm, covering monomer and dimer delay emission, we observe a linear power dependence, which would indicate a very slow delayed singlet generation mechanism. At 20 K, TADF seems very unlikely. We also obtained the fluence dependency in the 400-430 nm spectral window. Although noisy and rather pushing the limits of our detectivity, we again observe a linear dependency, supporting the assignment that this emission, peak at 420-425 nm is a monomolecular process.

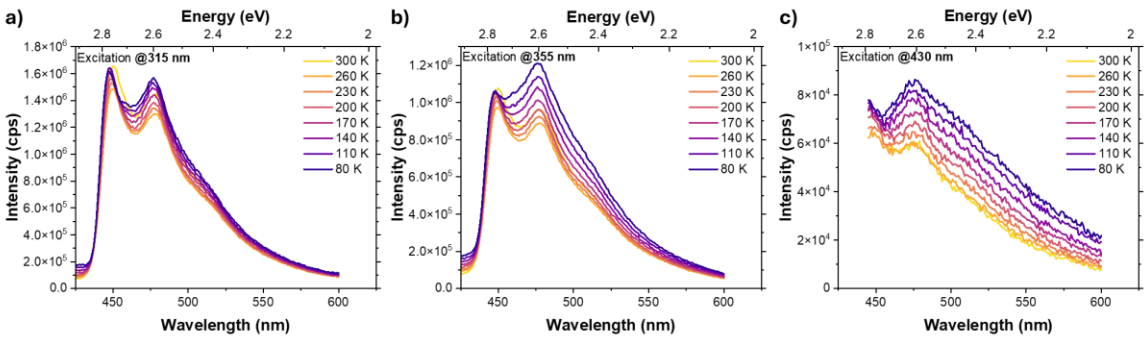

Fig S18. Temperature dependency of polystyrene guest-host film. PL of $HzTFEX_2$ doped into polystyrene guest-host films at 0.01% wt/wt in a range of temperatures. (a) λ_{ex} = 315 nm. (b) λ_{ex} = 355 nm. (c) λ_{ex} = 430 nm.

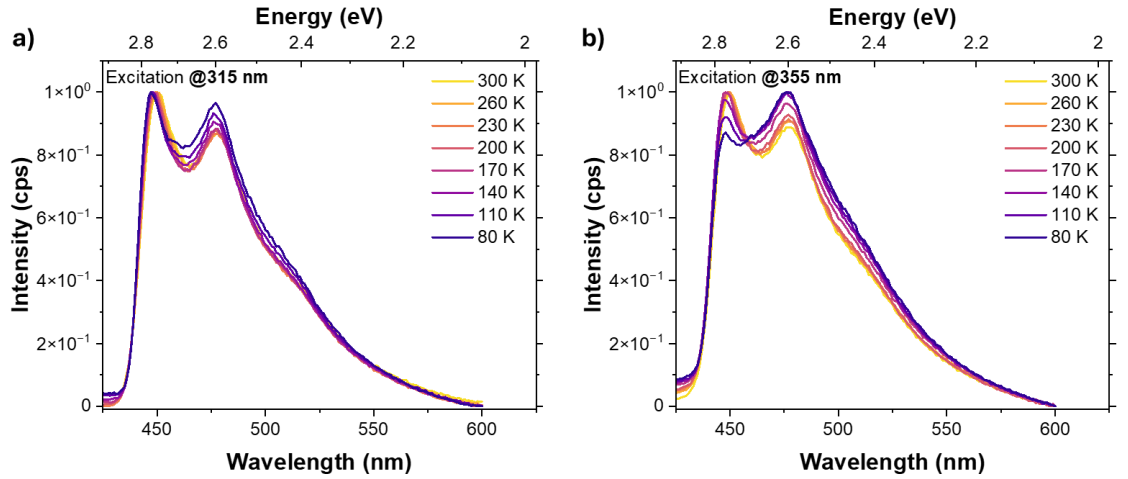

Fig S19. Temperature dependency of polystyrene guest-host film. Normalized PL of $HzTFEX_2$ doped into polystyrene guest-host films at 0.01% wt/wt in a range of temperatures. (a) λ_{ex} = 315 nm. (b) λ_{ex} = 355 nm.

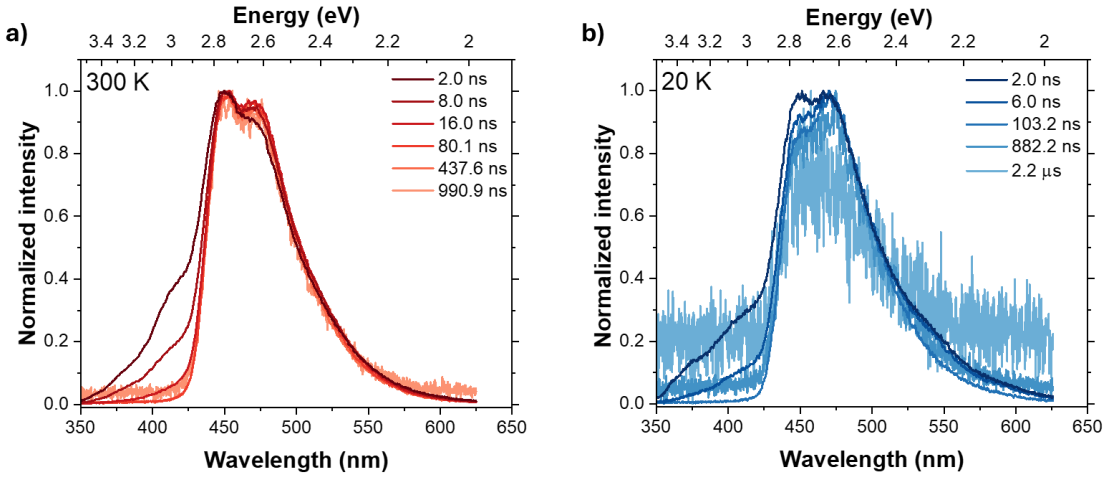

Fig S20. Time-resolved photoluminescence of polystyrene guest-host film. TRPL of $HzTFEX_2$ doped into polystyrene guest-host films at 0.01% wt/wt monitored at (a) 300 K and (b) 20 K. λ_{ex} = 355 nm.

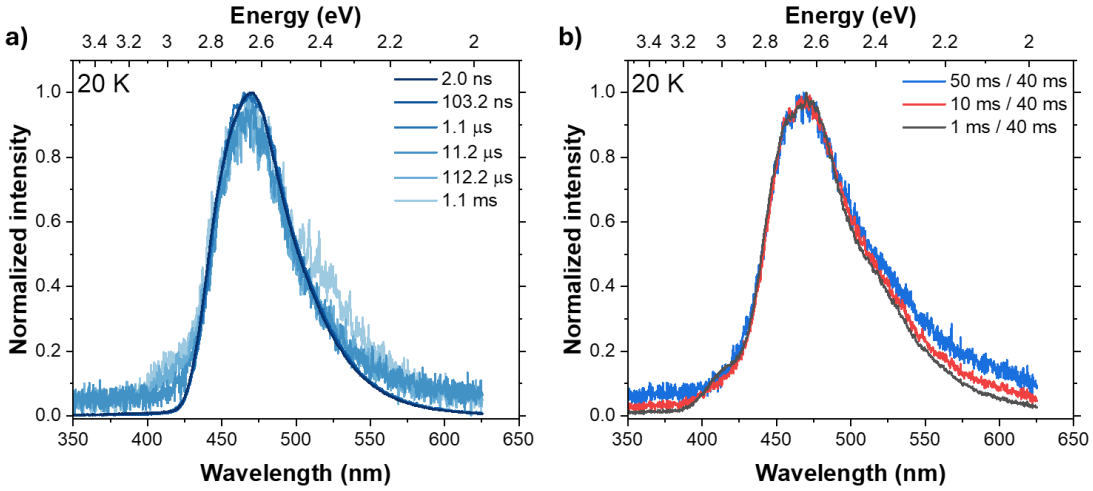

Fig S21. Time-resolved photoluminescence of polystyrene guest-host film. (a) TRPL and (b) phosphorescence curves of $HzTFEX_2$ doped into polystyrene guest-host films at 0.1% wt/wt monitored at 20 K. Legends indicated DT / IT used for spectra acquisition of phosphorescence. λ_{ex} = 355 nm.

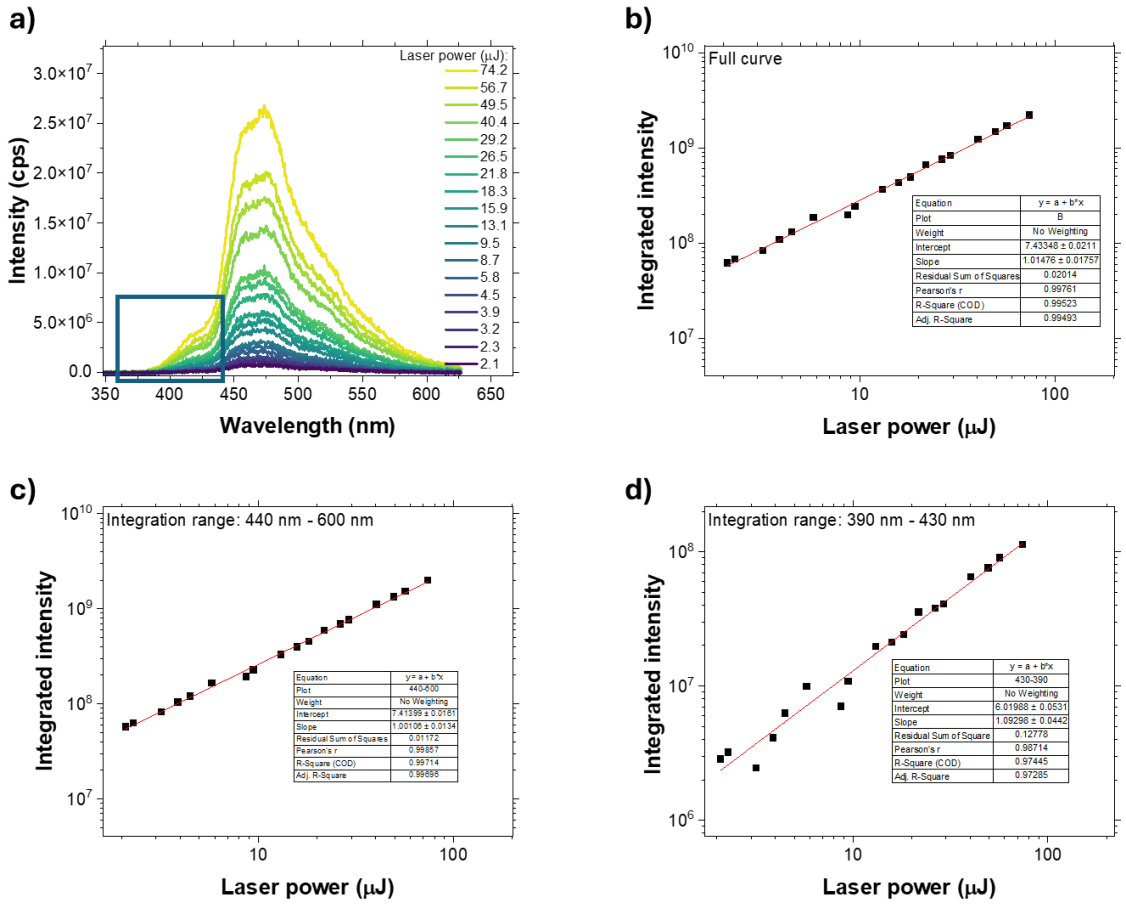

Fig S22. Dependency of PL with incident light intensity. (a) PL of $HzTFEX_2$ doped into polystyrene guest-host films at 0.1% wt/wt monitored at 20 K in a range of laser powers. DT = 300 µs and IT = 10 ms. (b, c and d) Integrated PL versus laser power on different parts of the emission spectra. Data were fitted with a linear equation. λ_{ex} = 337 nm

4.2. Zeonex

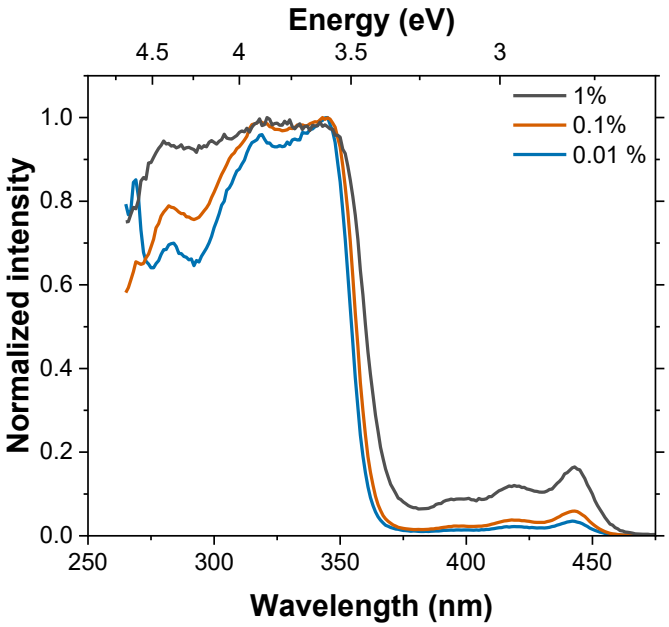

Fig S23. Excitation of Zeonex guest-host film. Excitation profile of $HzTFEX_2$ doped into Zeonex guest-host films monitored at room temperature in a range of concentrations (wt %/ wt %). Emission was monitored at 460 nm.

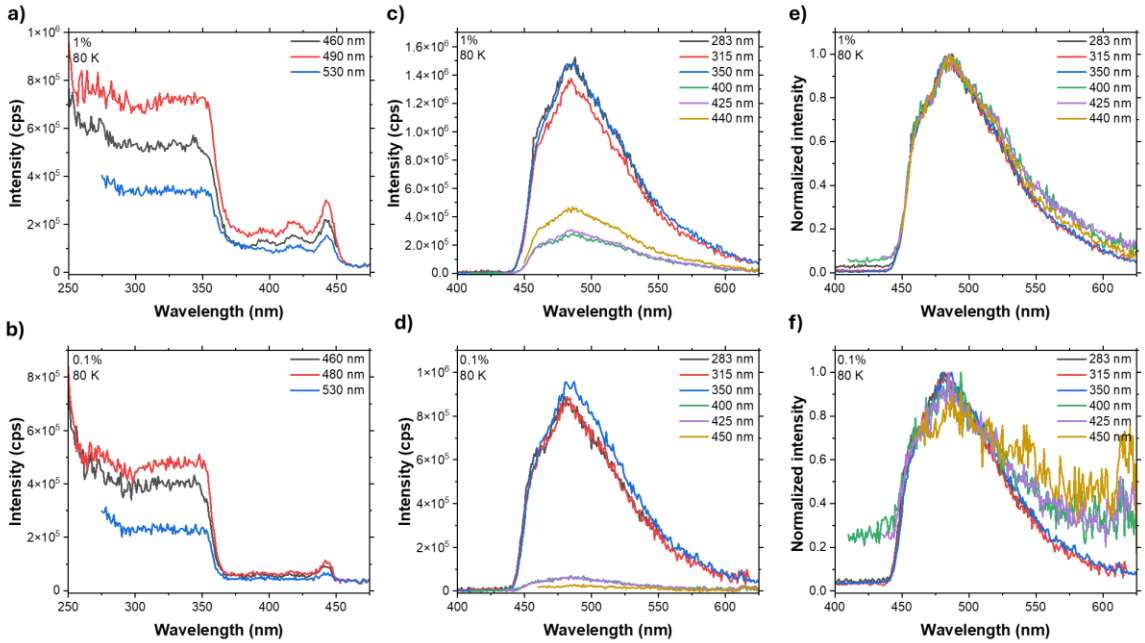

Fig 24. Photoluminescence of Zeonex guest-host film at low temperature. Excitation profile of $HzTFEX_2$ doped into Zeonex guest-host films monitored at 80 K at (a) 1% and (b) 0.1% wt/wt. Monitored wavelengths are indicated. PL of $HzTFEX_2$ doped into Zeonex guest-host films monitored at 80 K at (c,e) 1% and (d,f) 0.1% wt/wt. Excitation and monitored wavelengths are indicated.

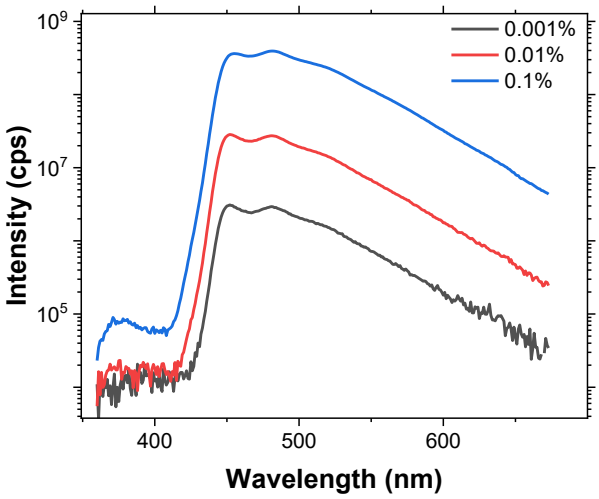

Fig 25. Photoluminescence of Zeonex guest-host film. PL of $HzTFEX_2$ doped into Zeonex guest-host films in a range of concentrations. λ_{ex} = 350 nm.

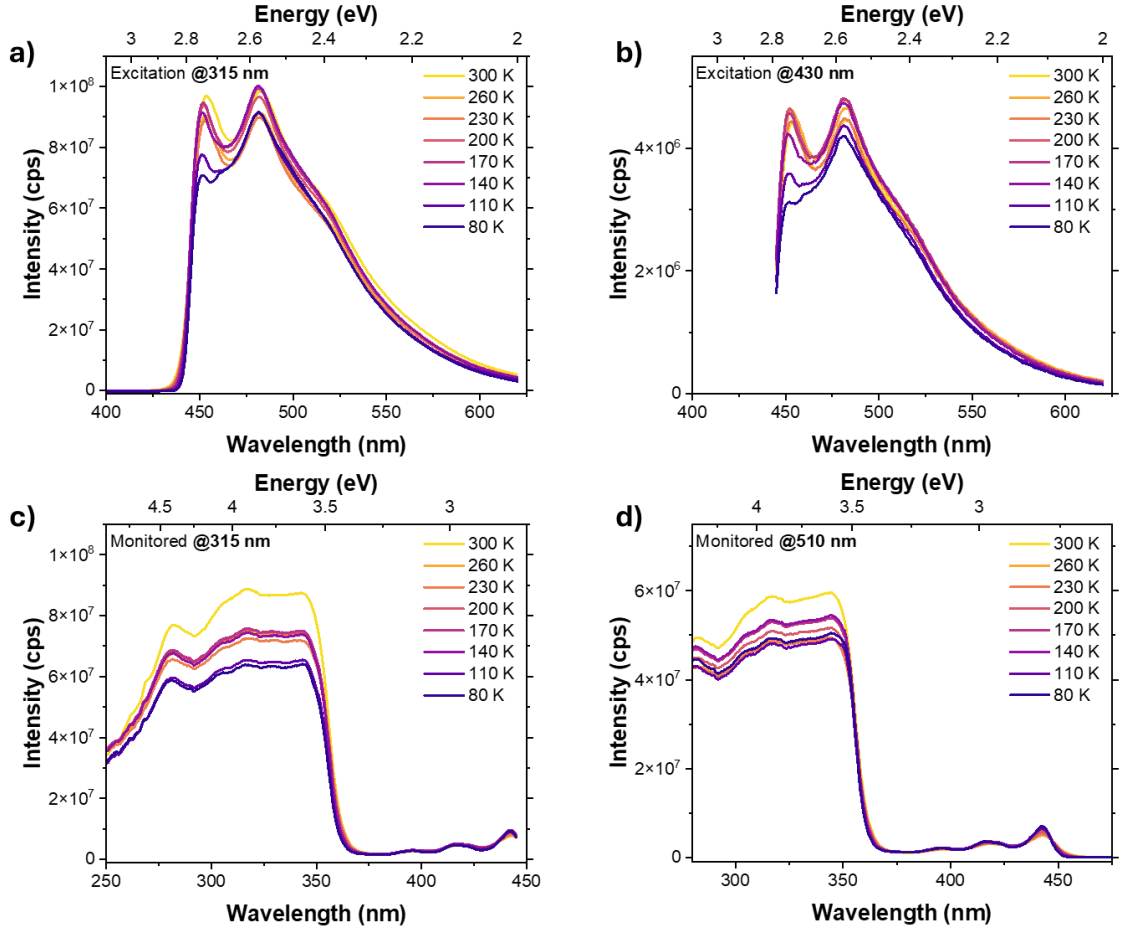

Fig S26. Temperature dependency of Zeonex guest-host film. PL of $HzTFEX_2$ doped into Zeonex guest-host films at 0.1% wt/wt in a range of temperatures. (a) λ_{ex} = 315 nm. (b) λ_{ex} = 430 nm. Excitation profile of $HzTFEX_2$ doped into Zeonex guest-host films at 0.1% wt/wt in a range of temperatures. (c) λ_{mon} = 460 nm. (d) λ_{mon} = 510 nm

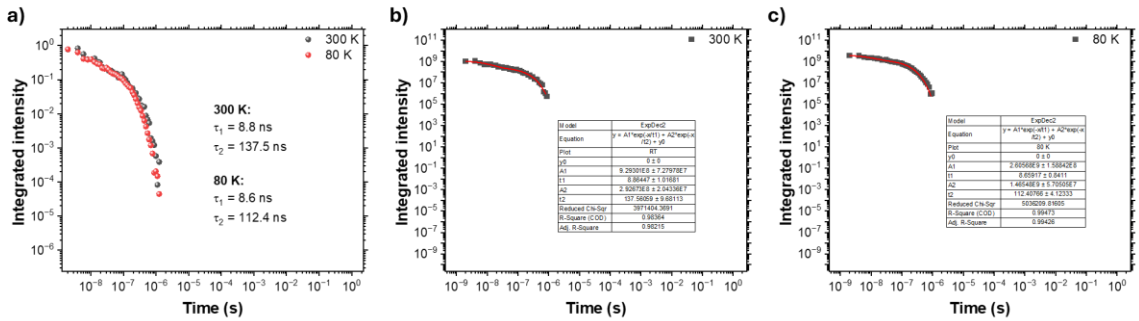

Fig 27. Time-resolved photoluminescence of Zeonex guest-host film. (a) Decay curves of $HzTFEX_2$ doped into Zeonex guest-host films at 0.001% wt/wt monitored at 300 K and 80 K. (b, c) Curves were fitted to a biexponential equation. λ_{ex} = 355 nm.

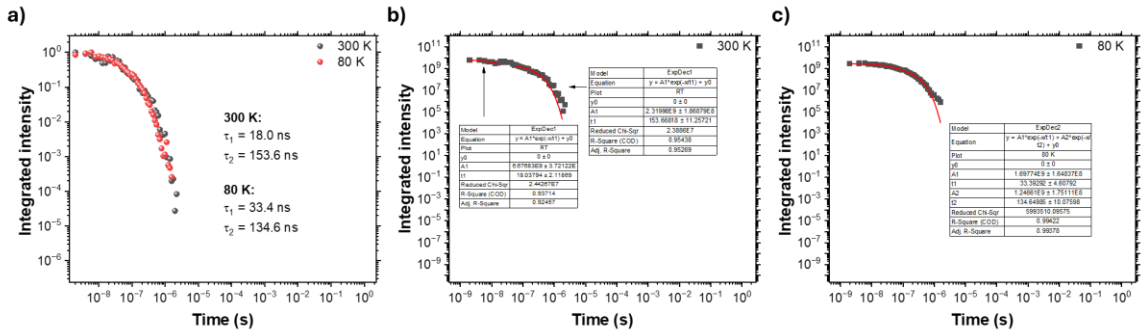

Fig 28. Time-resolved photoluminescence of Zeonex guest-host film. (a) Decay curves of $HzTFEX_2$ doped into Zeonex guest-host films at 0.1% wt/wt monitored at 300 K and 80 K. (b, c) Curves were fitted to a biexponential equation. λ_{ex} = 355 nm.

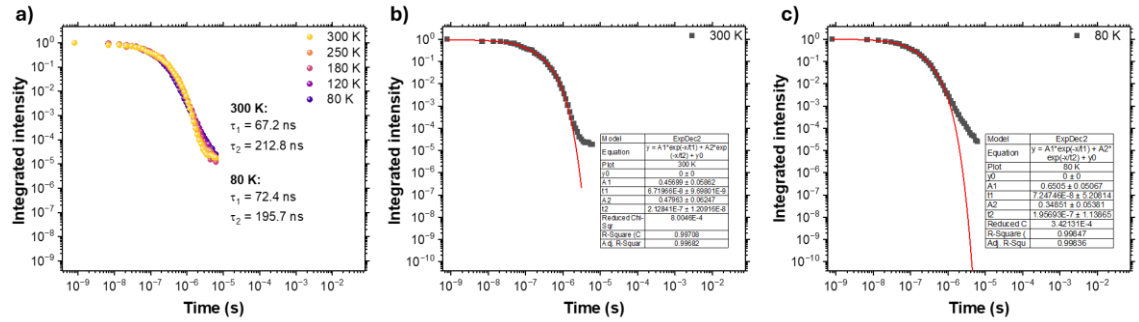

Fig S29. Time-resolved photoluminescence of Zeonex guest-host film. (a) Decay curves of $HzTFEX_2$ doped into Zeonex guest-host films at 1% wt/wt monitored in a range of temperatures. (b, c) Curves were fitted to a biexponential equation. λ_{ex} = 355 nm.

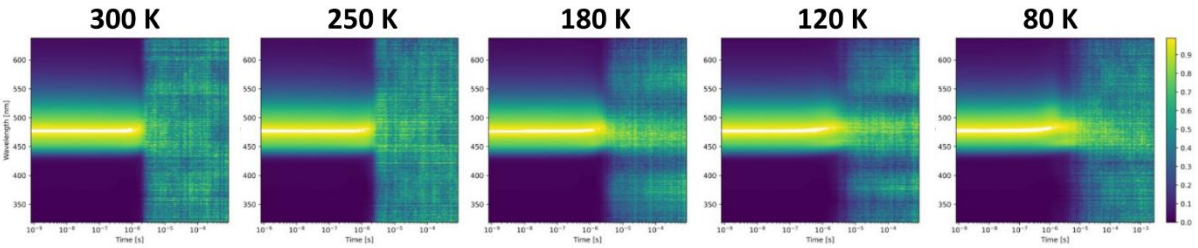

Fig S30. Time-resolved photoluminescence of Zeonex guest-host film. Contour plot of the decay of $HzTFEX_2$ doped into Zeonex guest-host films at 1% wt/wt monitored in a range of temperatures. λ_{ex} = 355 nm.

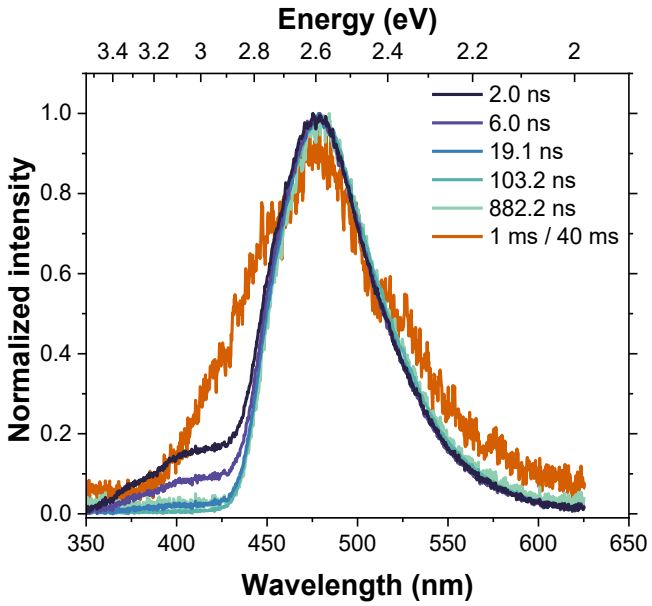

Fig S31. Time-resolved photoluminescence of Zeonex guest-host film. TRPL of $HzTFEX_2$ doped into Zeonex guest-host films at 0.01% wt/wt monitored at 20 K. λ_{ex} = 355 nm.

5. Temperature dependent solution measurements

5.1. Determination of solution temperature

It is usual for a discrepancy to exist between the temperature indicated by a temperature controller and the actual temperature of a solution inside a cryostat[1,2]. Given the nature of the measurements that were perfomed, we regarded that it was relevant to determine the temperature gap in our system. The temperature of toluene was varied to determine its freeing point according to our thermostat. Solution was left for 20 minutes at each temperature for stabilization. Toluene only became frozen when the thermostat indicated 145 K (Fig S32). Since the literature freezing point of toluene is 178 K[3], it was determined that there is a approximate 33 K difference between the temperature indicated by the thermostat and the real solution temperature.

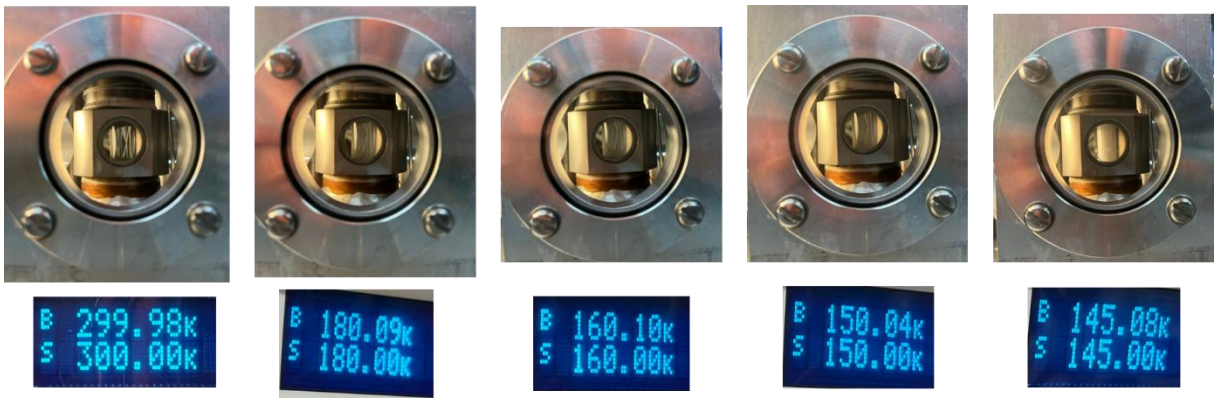

Fig S32. Temperature gap determination. Images of toluene in a range of temperatures.

5.2. 2-MeTHF

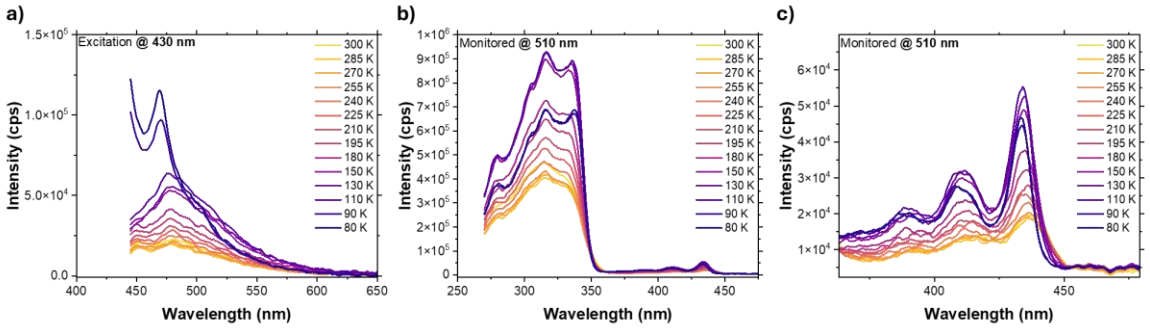

Figure 33. Temperature dependency of photoluminescence in 2-MeTHF solution. PL of $HzTFEX_2$ in 2-MeTHF 2μM air saturated solution monitored in a range of temperatures. (a) λ_{ex} = 430 nm. (b, c) Excitation profile monitoring emission at 510 nm in a range of temperatures.

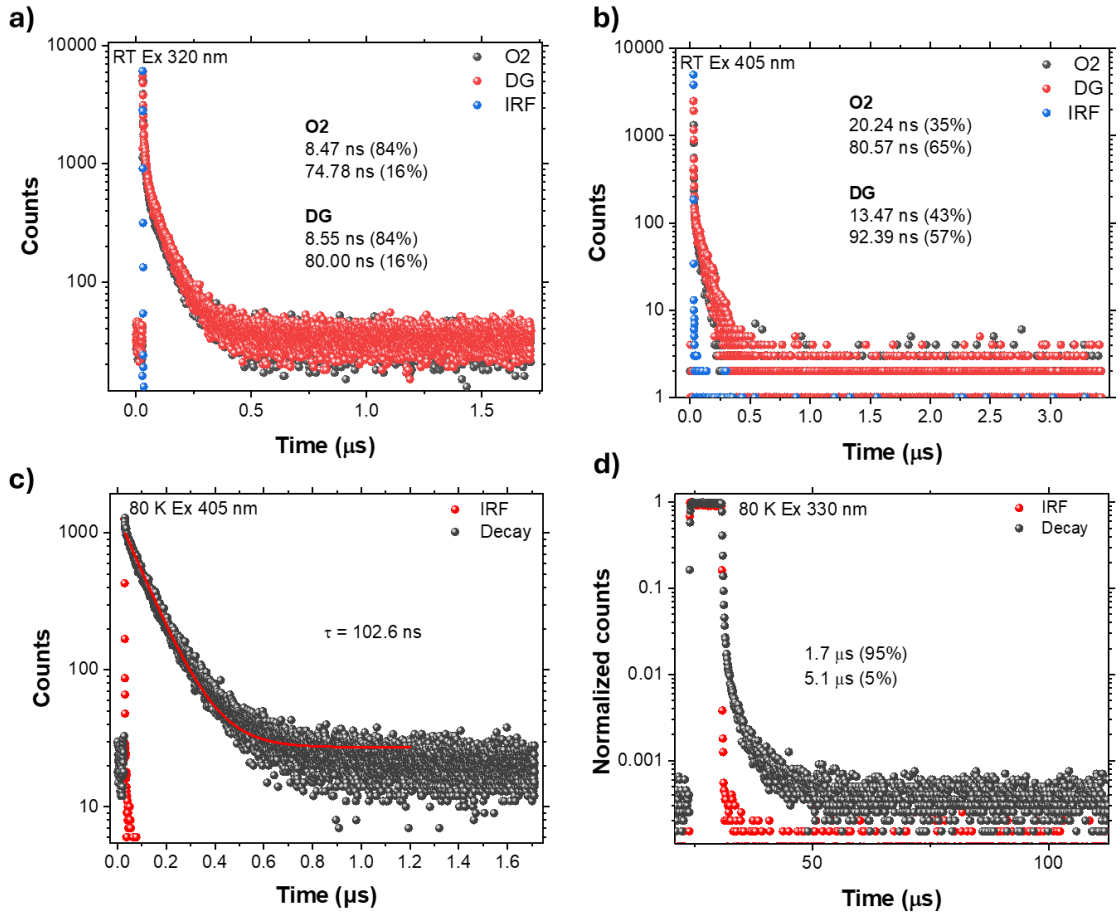

Fig S34. Time-resolved emission in 2-MeTHF solution. Decay curves of $HzTFEX_2$ in 2-MeTHF 2µM air saturated and degassed solution monitored at 450 nm at room temperature (a) λ_{ex} = 320 nm. (b) λ_{ex} = 405 nm. Decay curves of $HzTFEX_2$ in 2-MeTHF 2µM air saturated solution monitored at 450 nm at 80 K. (c) λ_{ex} = 405 nm. (d) λ_{ex} = 330 nm.

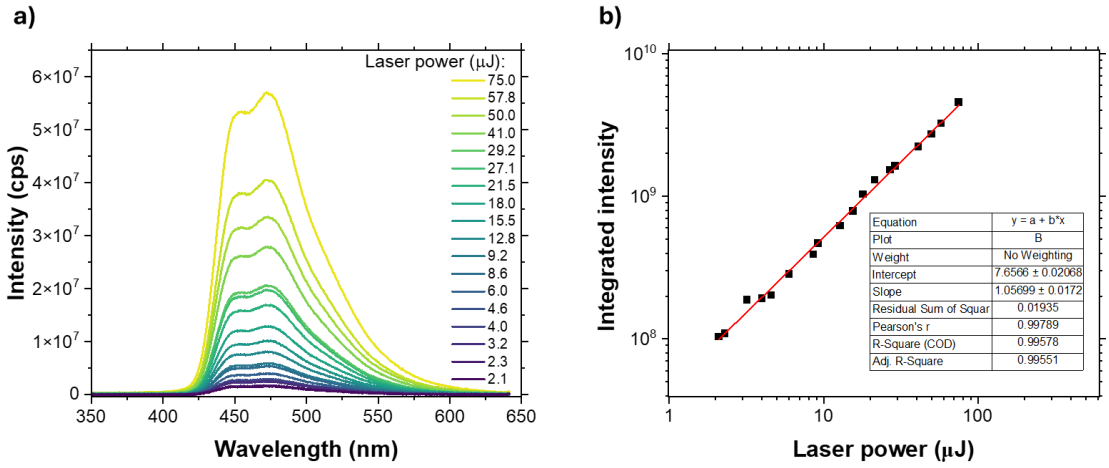

Fig S35. Dependency of PL with incident light intensity. (a) PL of $HzTFEX_2$ in 2-MeTHF 2 µM solution monitored at room temperature in a range of laser powers. DT = 1.4 µs and IT = 1.0 µs. (b) Integrated PL versus laser power. Data were fitted with a linear equation. λ_{ex} = 337 nm.

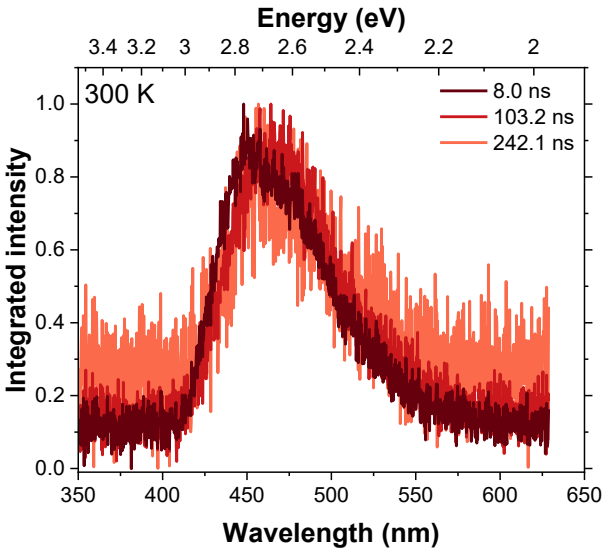

Fig S36. Time-resolved photoluminescence in 2-MeTHF solution. TRPL of $HzTFEX_2$ in 2-MeTHF 2 µM air saturated solution monitored at room temperature. λ_{ex} = 437 nm.

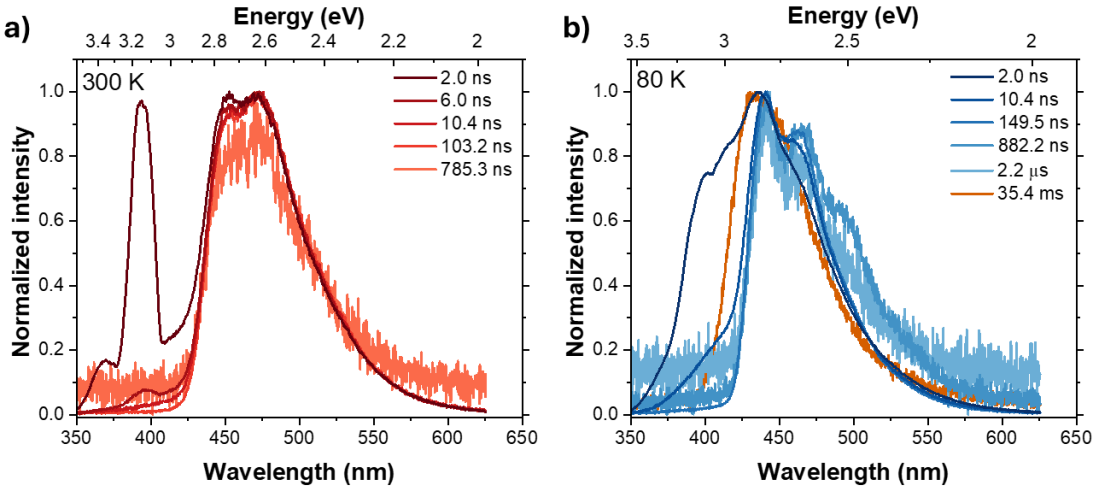

Fig S37. Time-resolved photoluminescence of 2-MeTHF solution. TRPL of $HzTFEX_2$ in 2-MeTHF 0.2µM air saturated solution monitored at (a) room temperature and (b) 80 K. λ_{ex} = 337 nm.

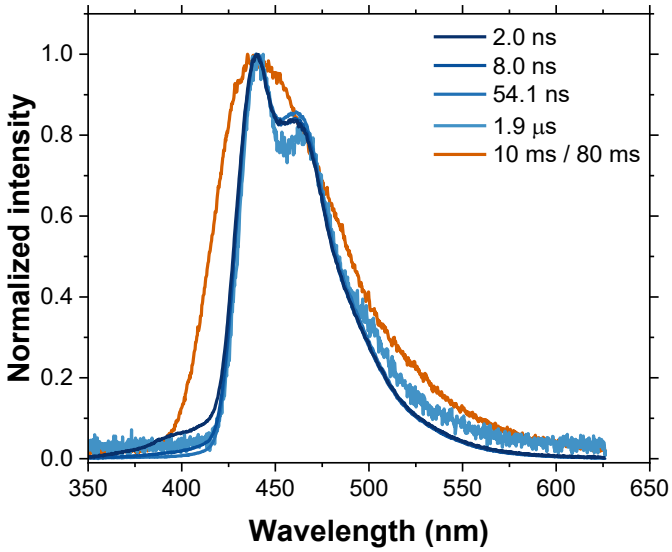

Fig S38. Time-resolved photoluminescence of 2-MeTHF solution. TRPL of $HzTFEX_2$ in 2-MeTHF 2µM air saturated solution monitored at 80 K. λ_{ex} = 355 nm.

5.3. MCH

Emission spectra in MCH are found to be both temperature and excitation energy dependent, more so than in other solvents (Figure S39). Exciting at 355 nm gives a high monomer component and well-resolved emission than 315 nm excitation. Around the freezing point (below 130 K measured in the cryostat) we observe a rather strange behaviour which is highly reproducible. At 130K, the solution is observed to be still fluid even after 1 hour held at temperature, but we observe a large blue shift of the emission band, to 434 nm (peak) and is highly structured and well resolved with 315 nm excitation, similar behaviour as in 2-MeTHF. Whereas at 355 nm excitation the spectra remain effectively unaffected except for a small intensity 434 nm component. Time-resolved spectra (Figure S41) show a fast decay of the 434 nm peak, relative to the peak at 450 nm. Concomitantly, the absorption band also blue shifts, and with the emission spectrum, clearly show almost all loss of dimer features. Upon dropping the temperature to 120 K, the solution freezes the emission becomes less resolved and a strong 'solution state like' monomer emission band (440nm 0-0 and 470 nm 0-1) reappearing with a 434 nm blue shoulder which is much more intense with 315 nm excitation. This 434 nm feature appears to correlate with excitation of the $S_0 \rightarrow S_N$ transition. As 355 nm excites an admixture of $S_0 \rightarrow S_N$ and $S_0 \rightarrow S_1$ transitions, we observe less of the 434 nm emission. At temperatures below 130 K (freeze point in the cryostat), the emission intensity grows very strongly, even though MCH does not form a clear glass. This again points to strong suppression of collisional dimer quenching of monomer states occurring in fluid solution. We have no answer for this complex behaviour in the highest polarizability solvent.

The excitation spectra monitored at both 460 nm and 510 nm (Figure S40) show a strong red edge 'spike' at 350 nm which disappears below 170 K and we also observe a red shifted $S_0 \rightarrow S_1$ transition having strong broad dimer absorption at around 435-450 nm, which disappears below 170 K leaving a lowest energy band at 425 nm and a residual sharp feature at 442 nm. In this region we can see that, from 230 K, the band tracks to higher energy reaching 425 nm at around the solvent freezing point with a small 442 nm band. The red edge 'spike' at 350 nm, and the strong red emission feature observed at 435-450 nm which disappears by 170 K, correlates with emission at 520 nm and potentially indicates that in high polarizable environments like MCH and in the single crystal, the 520 nm emitting dimer species has a distinct strong absorption spectrum at these wavelengths.

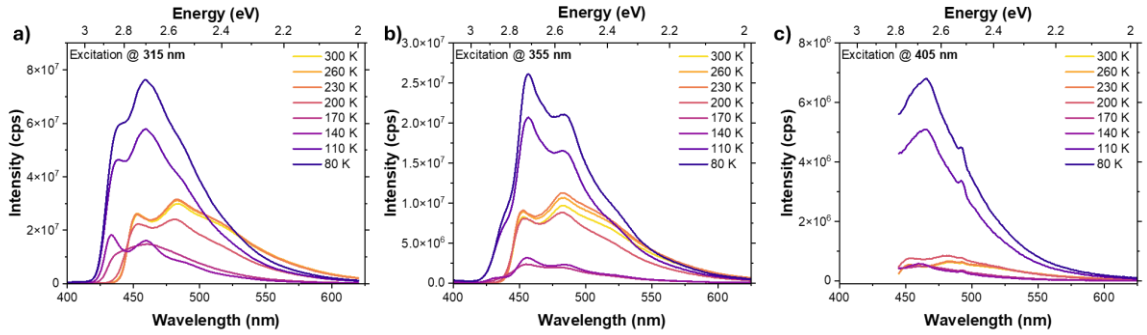

Fig S39. Temperature dependency of photoluminescence in MCH solution. PL of $HzTFEX_2$ in MCH 2μM air saturated solution monitored in a range of temperatures. (a) λ_{ex} = 315 nm. (b) λ_{ex} = 355 nm. (c) λ_{ex} = 405 nm.

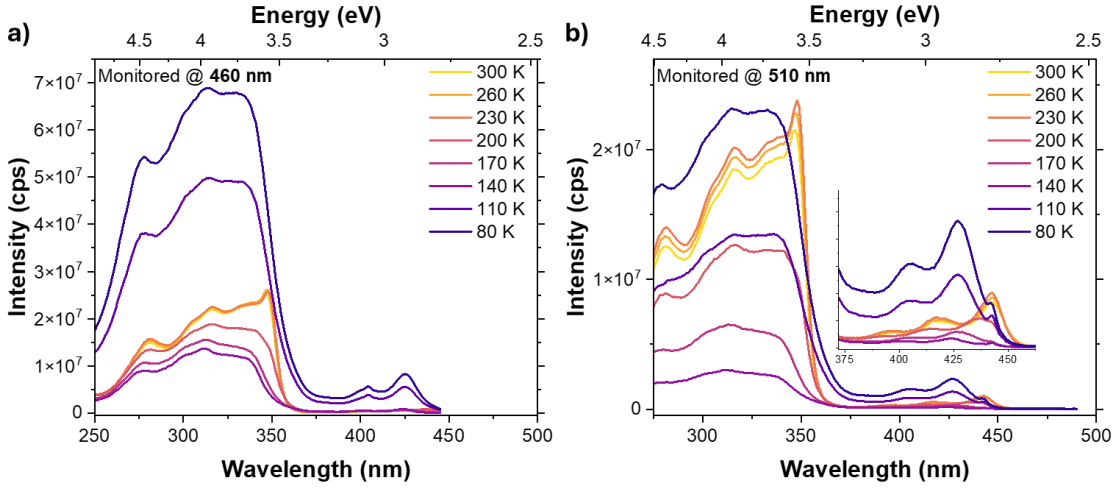

Fig S40. Temperature dependency of excitation in MCH solution. Excitation profile monitoring emission at (a) 460 nm and (b) 510 nm in a range of temperatures. Inset shows zoomed signal between 375 nm to 475 nm.

Time-resolved data do not provide many more clues. With 355 nm excitation (Figure S42) we see that we excite more dimer in the frozen state, at early times (2ns) we see $S_0 \leftarrow S_2$ emission and at late times broad emission from 500 nm to 650 nm, which we ascribe to DF and possible dimer phosphorescence. We also see very long-lived monomer emission at 450 nm, which must be delayed emission, most likely TTA. We do not see any emission below 450 nm after 10 ns. At 135 K, we do observe 434 nm emission at 6 ns combined with 450 nm emission. By 250 ns, we only observe 450 nm emission. We see clear monomer emission at 1 µs (450 nm 0-0, 475 nm 0-1), which lasts beyond 10 µs, implying slow collisional TTA. Collecting emission with delay and integration times of 1 ms and 40 ms, respectively, we see predominantly the same emission with a very weak 425 nm blue foot, much weaker than the similar feature seen in 2-MeTHF.

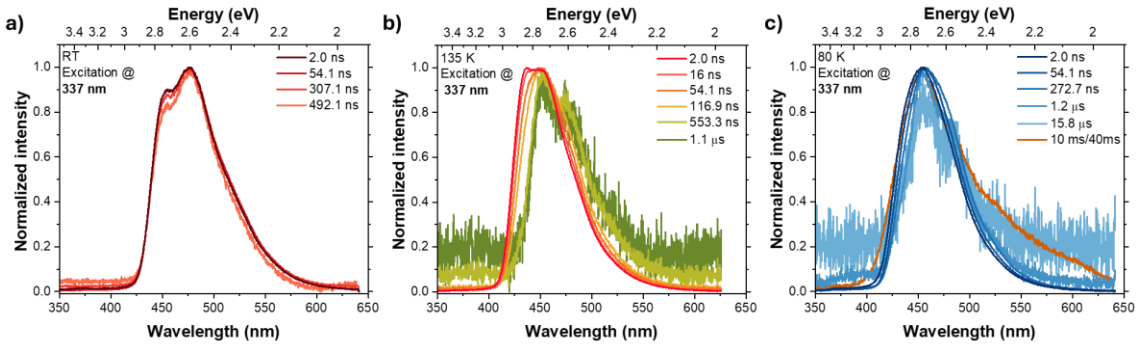

Fig S41. Time-resolved photoluminescence of MCH solution. TRPL of $HzTFEX_2$ in MCH 2µM air saturated solution monitored at (a) room temperature, (b) 135 K and (c) 80 K. λ_{ex} = 337 nm.

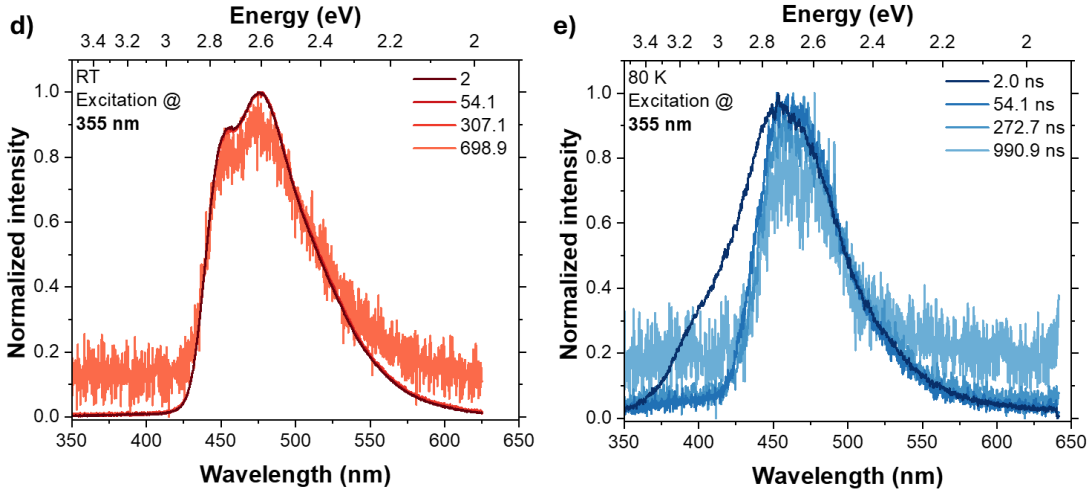

Fig S42. Time-resolved photoluminescence of MCH solution. TRPL of $HzTFEX_2$ in MCH 2µM air saturated solution monitored at (a) room temperature and (b) 80 K. λ_{ex} = 355 nm.

5.4. Toluene

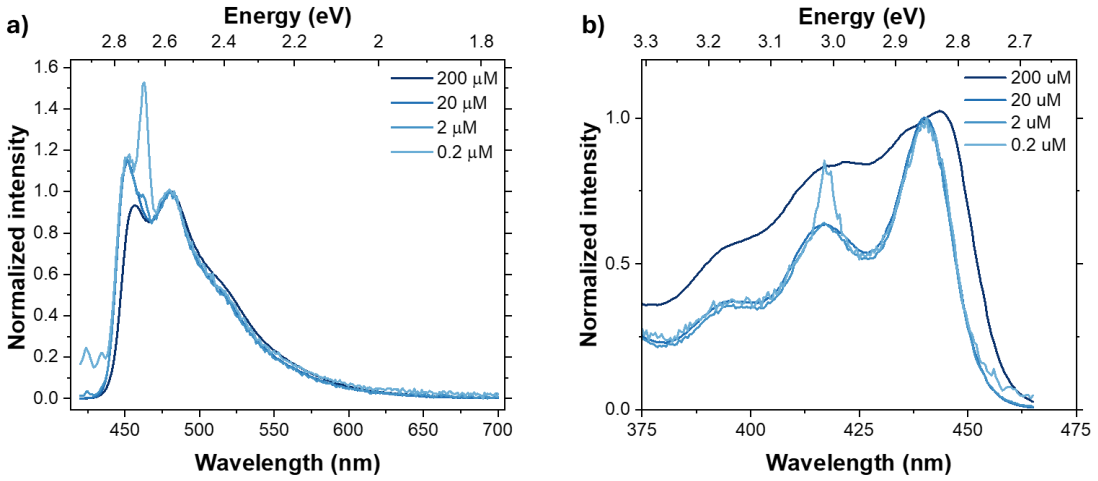

Fig S43. Concentration dependency of photoluminescence in toluene solution. (a) PL of $HzTFEX_2$ in toluene air saturated solution monitored at room temperature in a range of concentrations. Curves were normalized at 480 nm. λ_{ex} = 405 nm. (b) Excitation profile of $HzTFEX_2$ in toluene air saturated solution monitored at room temperature in a range of concentrations. PL was monitored at 480 nm. Curves were normalized at 440 nm.

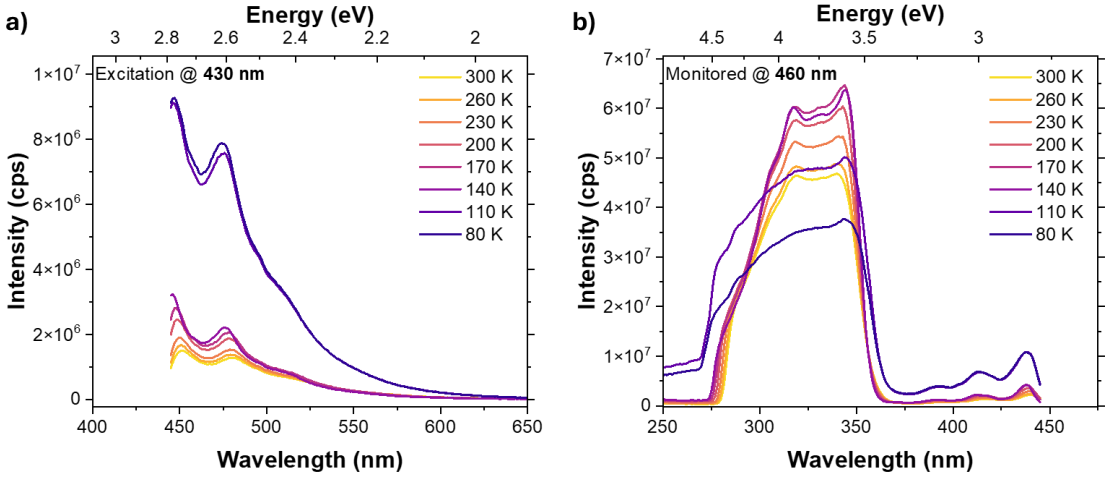

Fig S44. Temperature dependency of photoluminescence in toluene solution. (a) PL of $HzTFEX_2$ in toluene 2µM air saturated solution monitored in a range of temperatures. λ_{ex} = 430 nm. (b) Excitation profile monitoring emission at 460 nm in a range of temperatures.

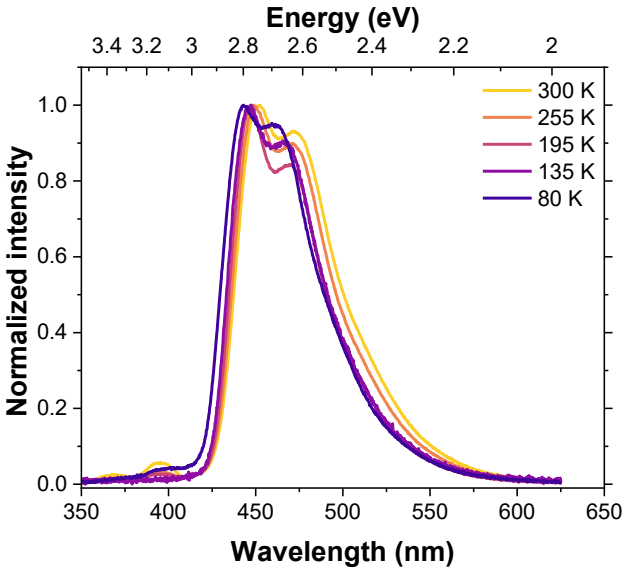

Fig S45. Temperature dependency of photoluminescence in toluene solution. Prompt emission of $HzTFEX_2$ in toluene 2 μM solution monitored in a range of temperatures. λ_{ex} = 355 nm.

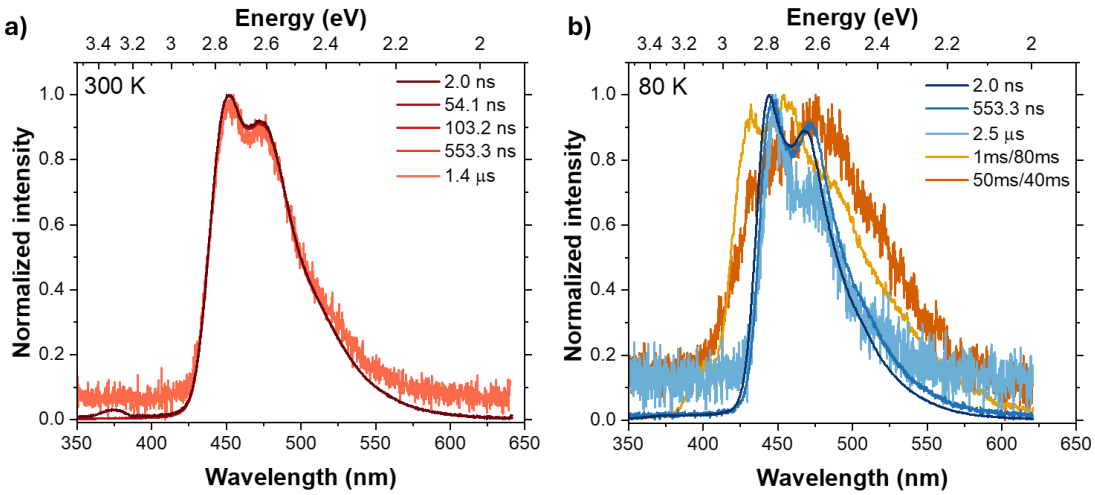

Fig S46. Time-resolved luminescence in toluene solution. TRPL of $HzTFEX_2$ in toluene 2μM air saturated solution monitored at (a) room temperature and (b) 80 K. λ_{ex} = 337 nm.

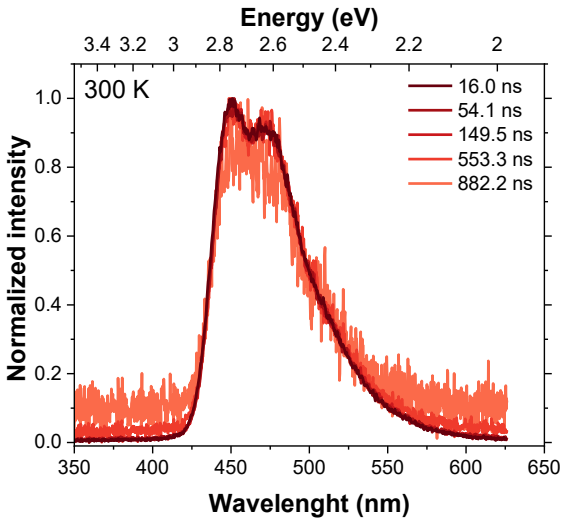

Fig S47. Time-resolved photoluminescence in toluene solution. TRPL of $HzTFEX_2$ in toluene 2 µM air saturated solution monitored at room temperature. λ_{ex} = 437 nm.

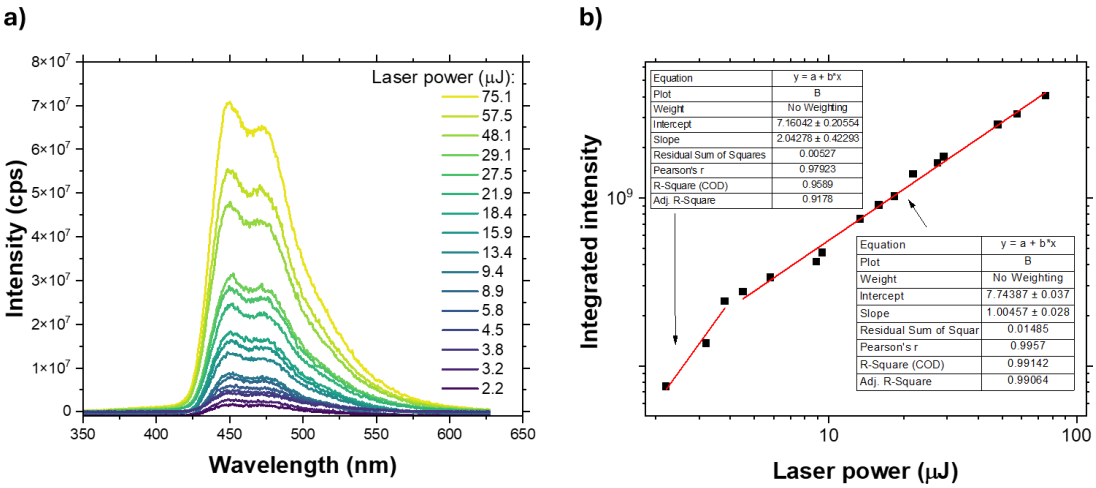

Fig S48. Dependency of PL with incident light intensity. (a) PL of $HzTFEX_2$ in toluene 2 µM solution monitored at room temperature in a range of laser powers. DT = 2.5 µs and IT = 10 µs. (b) Integrated PL versus laser power. Data were fitted with a linear equation. λ_{ex} = 337 nm.

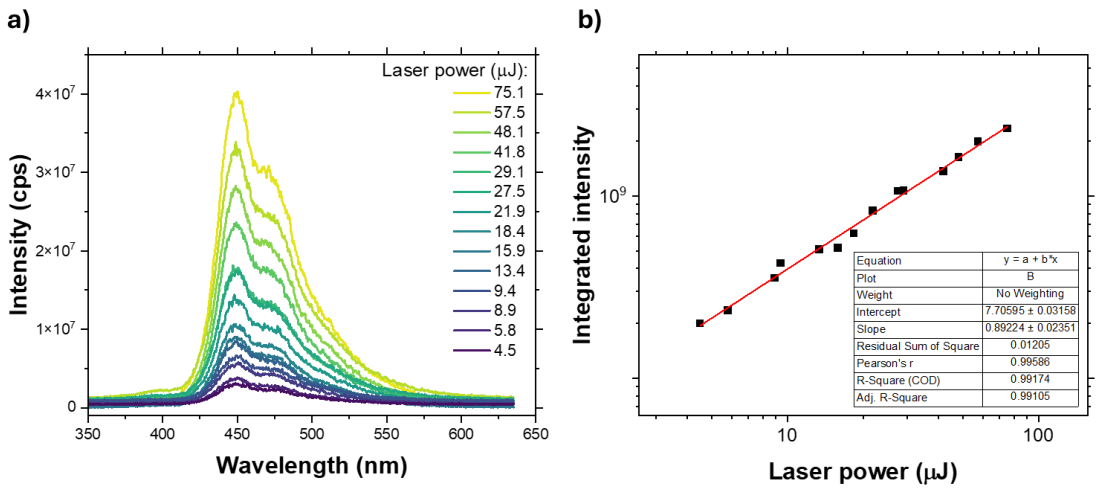

Fig S49. Dependency of PL with incident light intensity. (a) PL of $HzTFEX_2$ in toluene 2 μM solution monitored at 80 K in a range of laser powers. DT = 3.0 μs and IT = 10 μs. (b) Integrated PL versus laser power. Data were fitted with a linear equation. λ_{ex} = 337 nm.

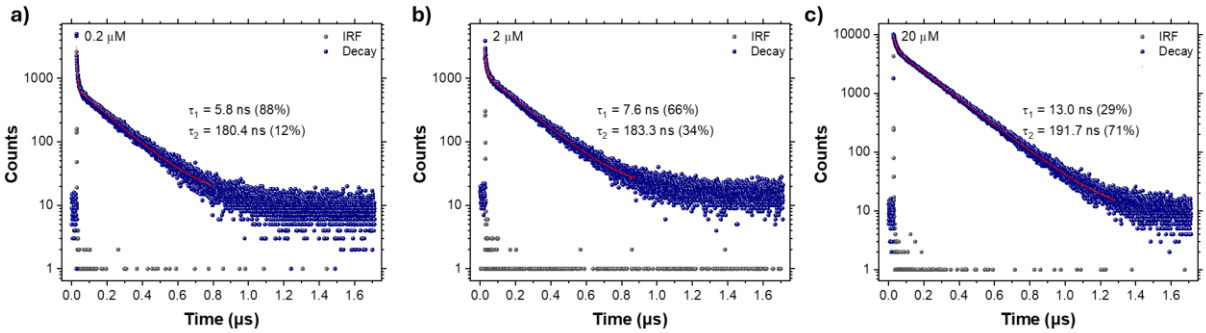

Fig S50. Concentration dependency of photoluminescence in toluene solution. Decay curve of $HzTFEX_2$ in toluene solution monitored at room temperature at (a) 0.2 μM, (b) 2 μM and (c) 20 μM. λ_{ex} = 405 nm. Decay was collected at 450 nm.

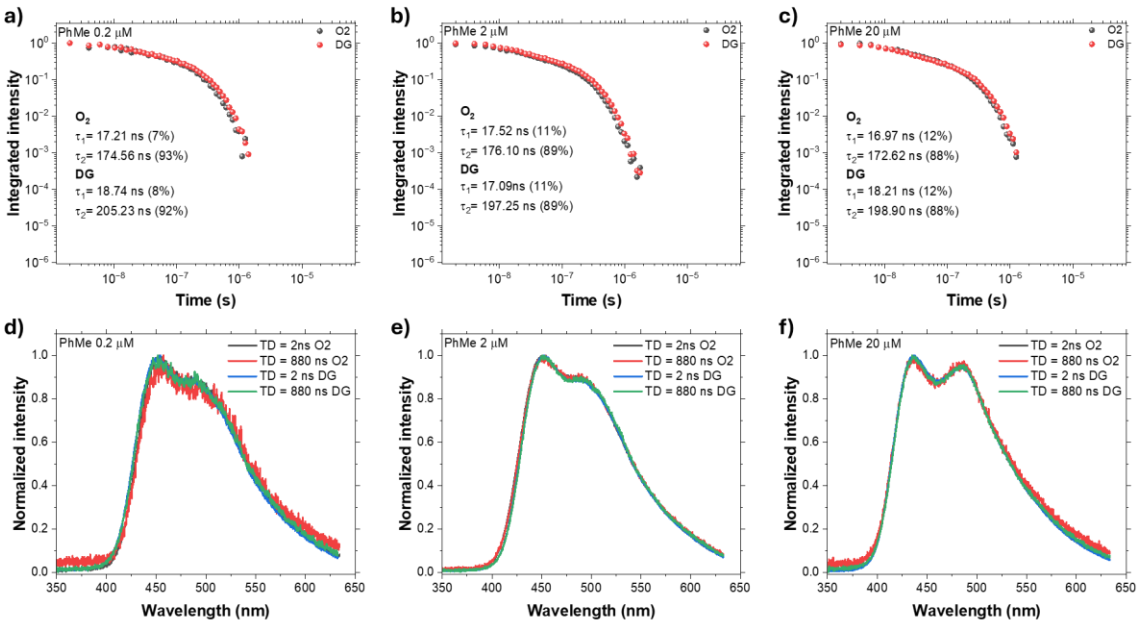

Fig S51. Impact of O_2 in the photoluminescence in toluene solution. (a, b and c) Decay curves of $HzTFEX_2$ in toluene saturated and degassed solution at different concentrations. Decay profiles were fitted to a biexponential equation. (d, e and f) TRPL curves of $HzTFEX_2$ in toluene saturated and degassed solution at different concentrations. λ_{ex} = 355 nm.

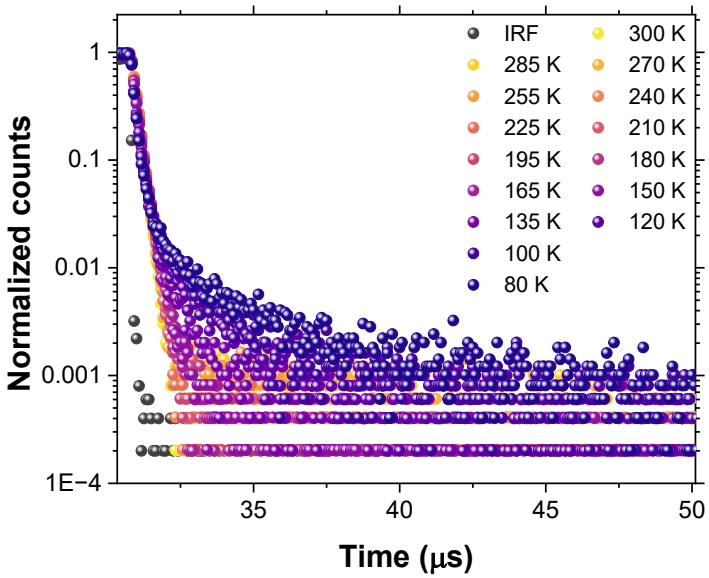

Fig S52. Temperature dependency of photoluminescence in toluene solution. Decay curve of $HzTFEX_2$ in toluene 2 µM solution monitored in a range of temperatures. λ_{ex} = 330 nm. Decay was monitored at 450 nm.

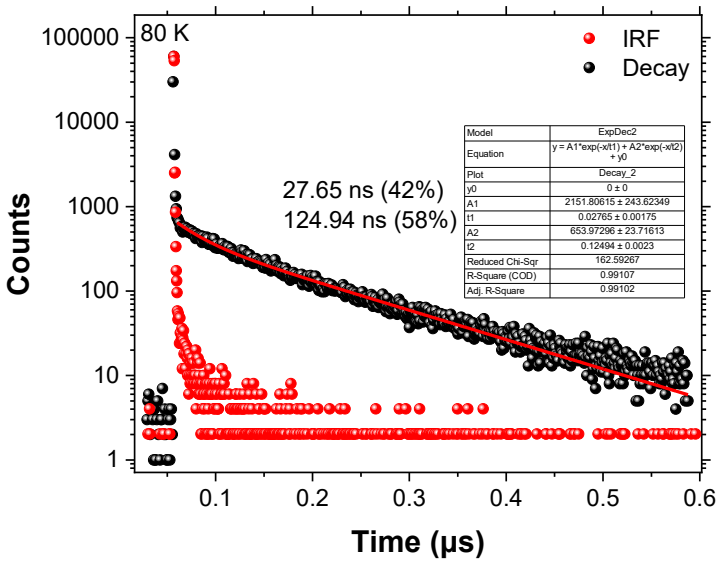

Fig S53. Behaviour of fluorescence at 80 K in toluene. Decay curve of $HzTFEX_2$ in toluene 2 µM solution at 80 K. Curve was fitted to biexponential equation. λ_{ex} = 405 nm. Decay was collected at 450 nm.

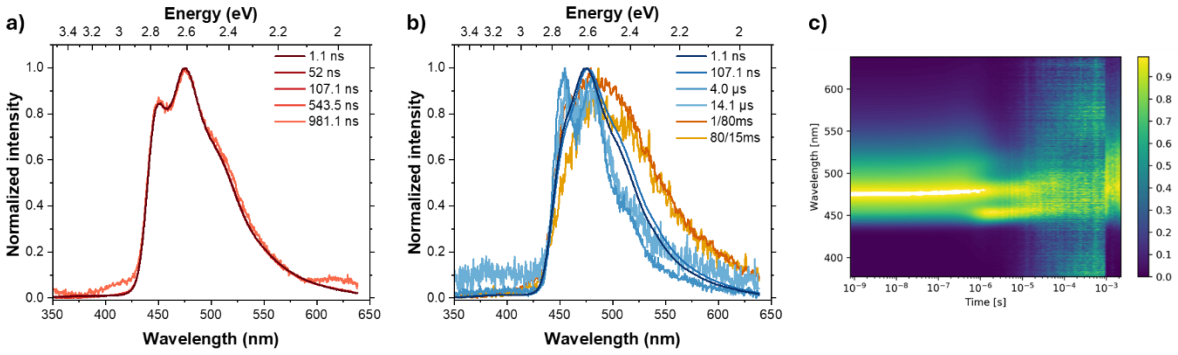

Fig S54. Time-resolved photoluminescence in toluene solution. TRPL of $HzTFEX_2$ in toluene 20 µM air saturated solution monitored at (a) room temperature and (b) 80 K. λ_{ex} = 355 nm. (c) Contour plot of the decay at 80 K.

5.5. Acetonitrile

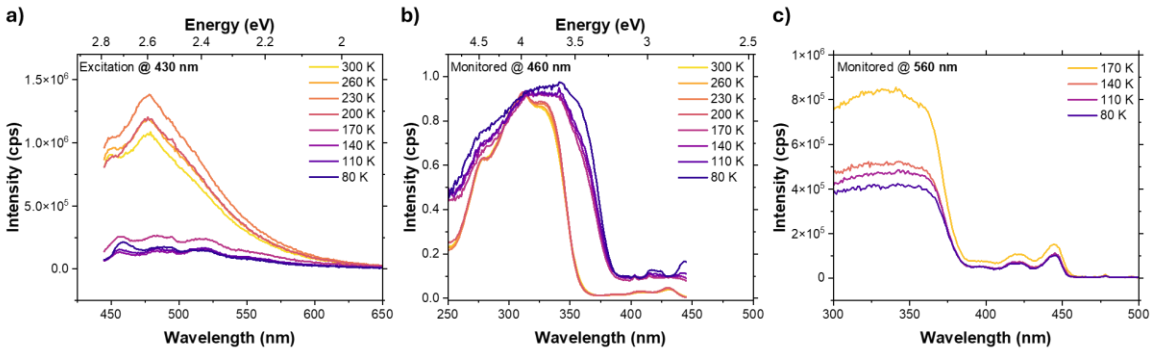

Fig S55. Temperature dependency of photoluminescence in acetonitrile solution. (a) PL of $HzTFEX_2$ in acetonitrile 2μM air saturated solution monitored in a range of temperatures. λ_{ex} = 430 nm. Excitation profile monitoring emission at (b) 460 nm and (c) in a range of temperatures. Signal of (b) was corrected by PL intensity.

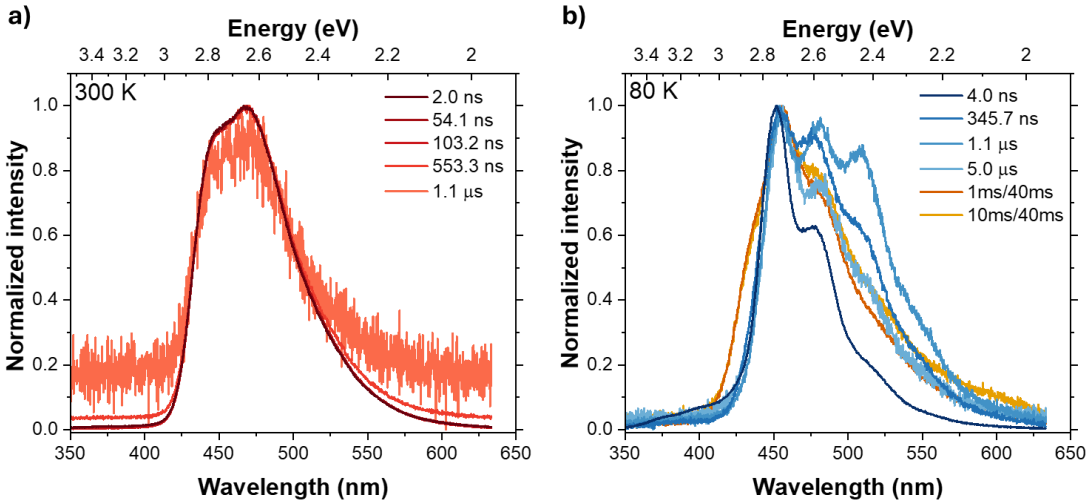

Fig S56. Time-resolved luminescence in acetonitrile solution. TRPL of $HzTFEX_2$ in acetonitrile 2 μM air saturated solution monitored at (a) room temperature and (b) 80 K. λ_{ex} = 337 nm.

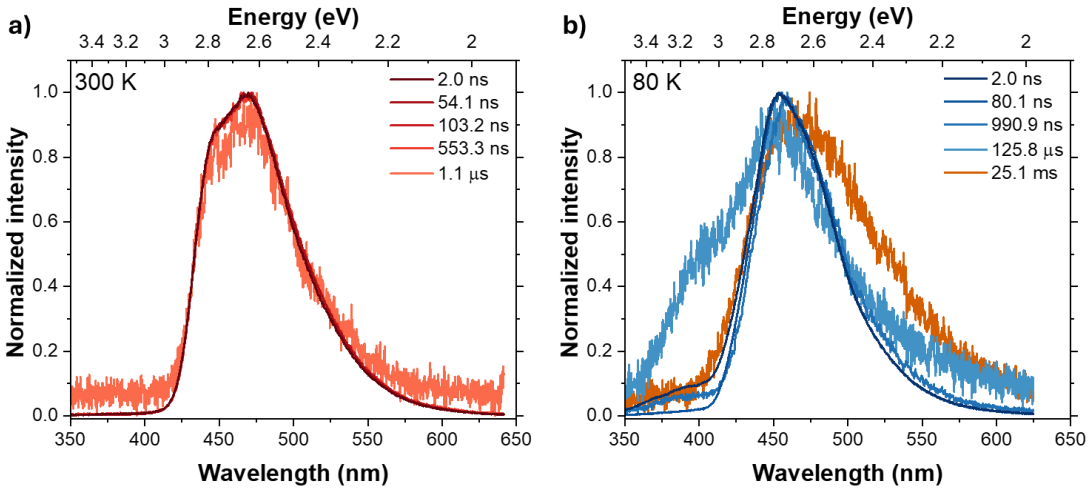

Fig S57. Time-resolved luminescence in acetonitrile solution. TRPL of $HzTFEX_2$ in acetonitrile 0.2 µM air saturated solution monitored at (a) room temperature and (b) 80 K. λ_{ex} = 337 nm.

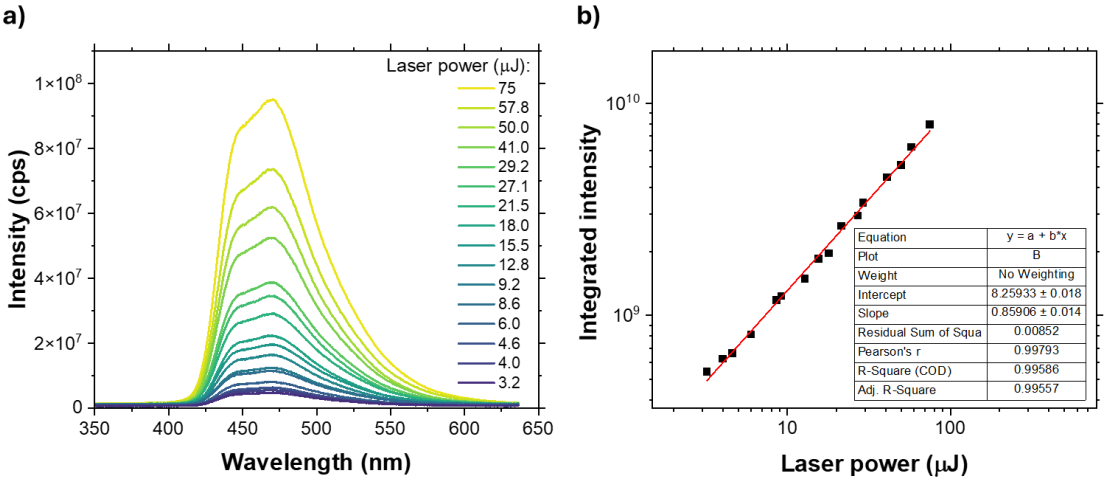

Fig S58. Dependency of PL with incident light intensity. (a) PL of $HzTFEX_2$ in acetonitrile 2 µM solution monitored at room temperature in a range of laser powers. DT = 1.7 µs and IT = 1.0 µs. (b) Integrated PL versus laser power. Data were fitted with a linear equation. λ_{ex} = 337 nm.

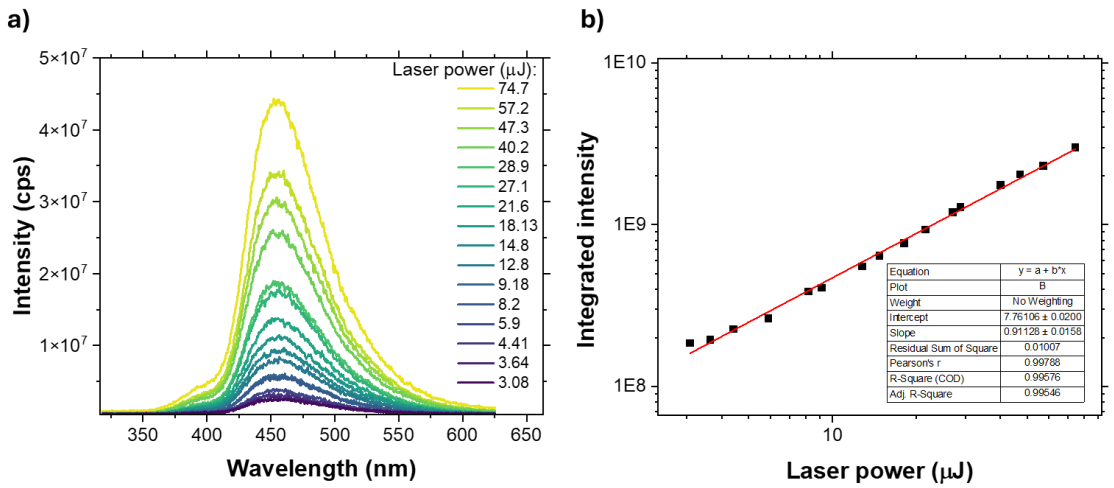

Fig S59. Dependency of PL with incident light intensity. (a) PL of $HzTFEX_2$ in acetonitrile 2 µM solution monitored at 80 K in a range of laser powers. DT = 10 µs and IT = 100 µs. (b) Integrated PL versus laser power. Data were fitted with a linear equation. λ_{ex} = 337 nm.

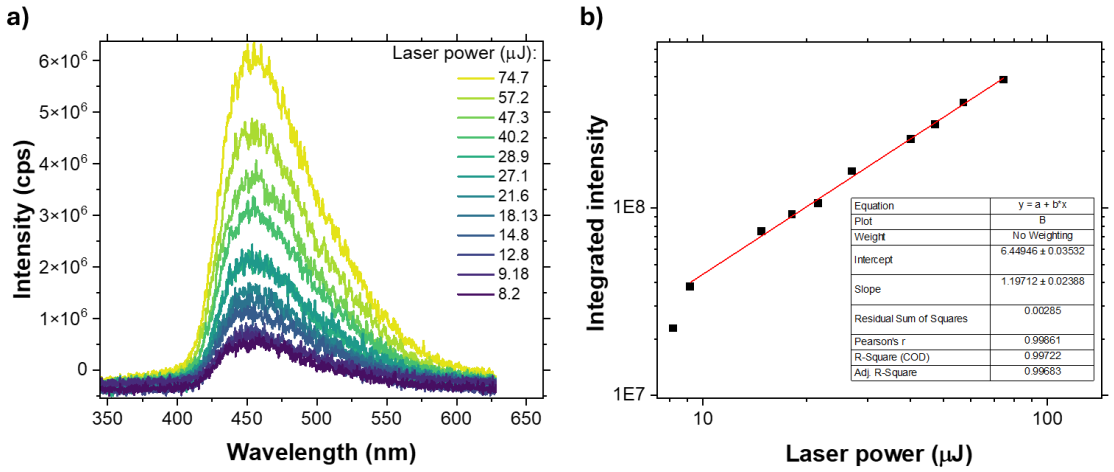

Fig S60. Dependency of PL with incident light intensity. (a) PL of $HzTFEX_2$ in acetonitrile 2 µM solution monitored at 80 K in a range of laser powers. DT = 10 µs and IT = 500 µs. (b) Integrated PL versus laser power. Data were fitted with a linear equation. λ_{ex} = 337 nm.

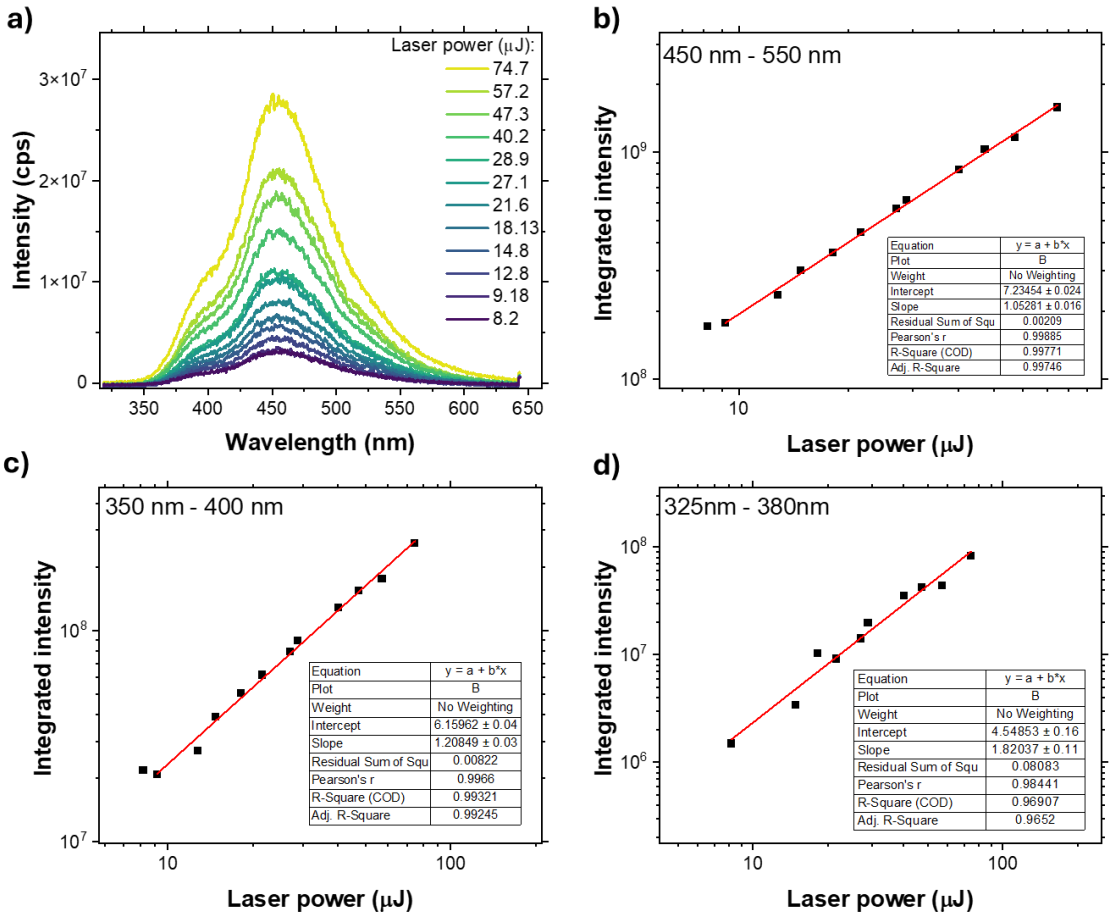

Fig S61. Dependency of PL with incident light intensity. (a) PL of $HzTFEX_2$ in acetonitrile monitored at 80 K in in acetonitrile 0.2 µM air saturated solution a range of laser powers. DT = 10 µs and IT = 100 µs. (b, c and d) Integrated PL versus laser power on different parts of the emission spectra. Data were fitted with a linear equation. λ_{ex} = 337 nm.

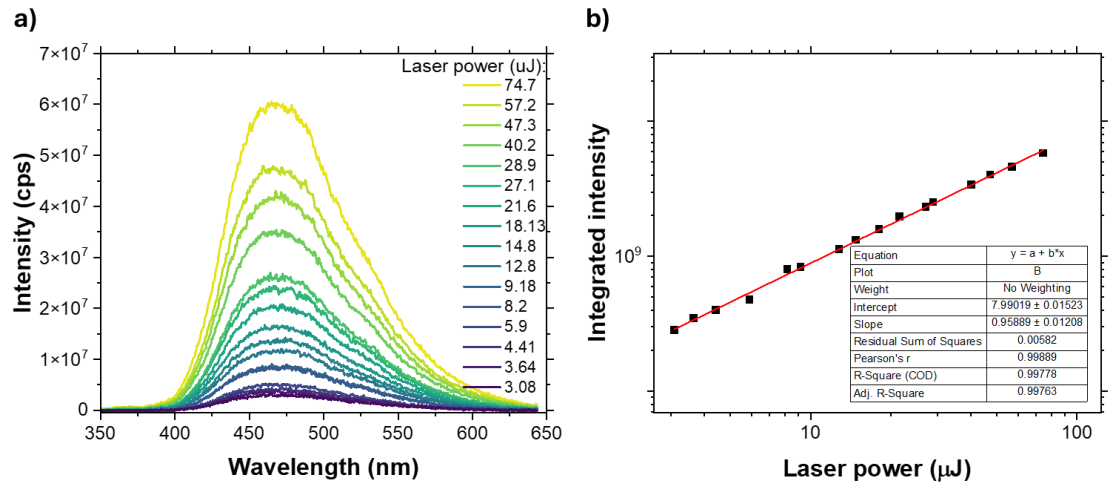

Fig S62. Dependency of PL with incident light intensity. (a) PL of $HzTFEX_2$ in acetonitrile 0.2 µM solution monitored at 80 K in a range of laser powers. DT = 1 ms and IT = 80 ms. (b) Integrated PL versus laser power. Data were fitted with a linear equation. λ_{ex} = 337 nm.

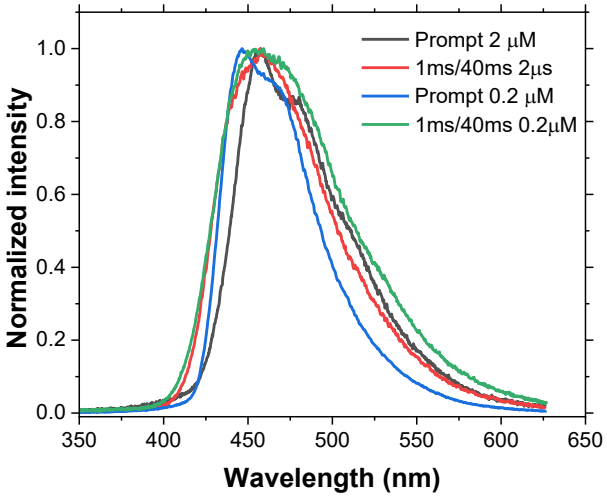

Fig S63. Concentration dependency of photoluminescence in acetonitrile solution. TRPL curves of $HzTFEX_2$ in 2 μM and 0.2 μM acetonitrile solution monitored at 80 K depicting prompt emission and emission acquired with DT=1 ms and IT=40 ms. λ_{ex} = 355 nm.

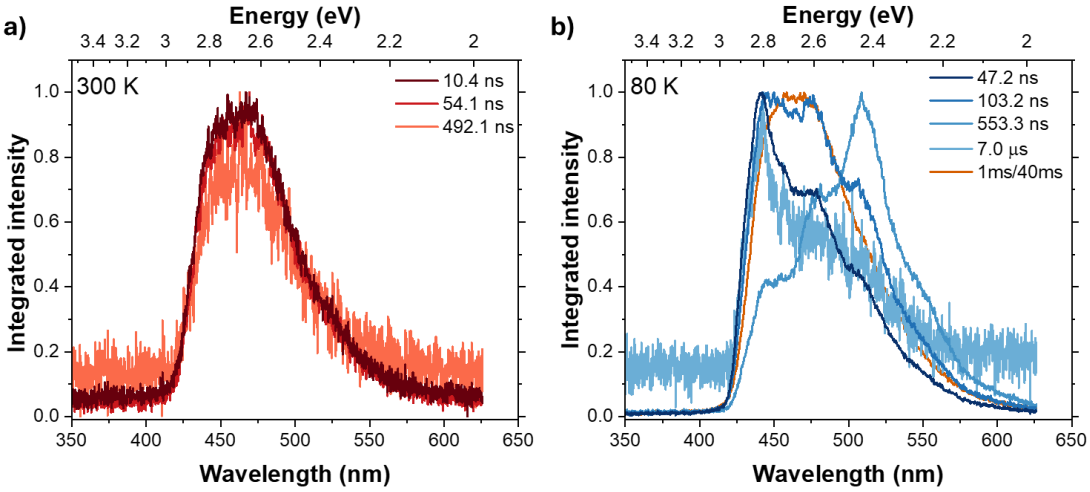

Fig S64. Time-resolved luminescence in acetonitrile solution. TRPL of $HzTFEX_2$ in acetonitrile 2 μM air saturated solution monitored at (a) room temperature and (b) 80 K. λ_{ex} = 437 nm.

6. Evidence of phosphorescence

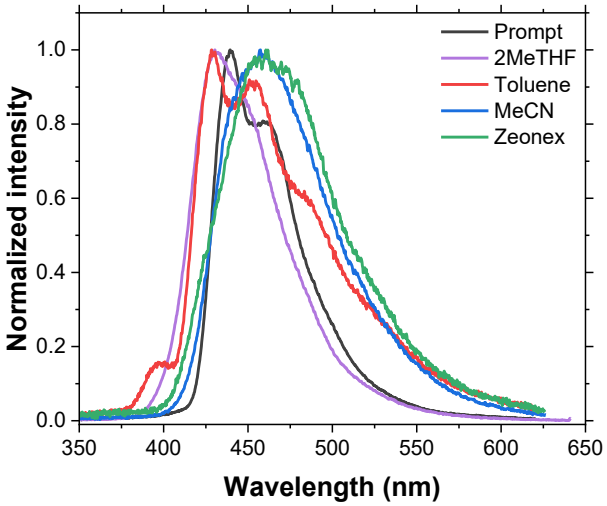

Fig S65. Phosphorescence of HzTFEX$_2$. TRPL of HzTFEX$_2$ in a range of environments depicting long lived emission (>1ms). Prompt was acquired in 2-MeTHF 2 μM solution monitored at 80 K with DT = 2.0 ns. Solution curves were acquired in 2 μM solution of the respective solvent monitored at 80 K with DT = 1 ms and IT = 40 ms. Zeonex curve was acquired with a 0.1% guest-host film monitored at 80 K with DT = 1 ms and IT = 40 ms. λ_{ex} = 355 nm.

7. Theoretical calculations

Table S2. Excited states of HzTFEX$_2$ at the optimized S_1 geometry.

State	Excitation energy (eV)	*f*	Character	Configuration
S_1	2.2899	0.0119	π-π*	HOMO → LUMO
S_2	3.0383	0.0032	n-π*	HOMO–4 → LUMO
S_3	3.1025	0.0015	n-π*	HOMO–6 → LUMO
S_4	3.5835	0.3870	n-π*, π-π*(CT)	HOMO–7 → LUMO, HOMO–1 → LUMO
S_5	3.6291	0.7745	π-π*(CT), n-π*	HOMO–1 → LUMO, HOMO–7 → LUMO,
S_6	3.8267	0.0116	π-π*(CT)	HOMO–2 → LUMO
S_7	3.8789	0.0664	π-π*(CT)	HOMO–3 → LUMO
S_8	3.9215	0.0228	π-π*, n-π*	HOMO → LUMO+1, HOMO–4 → LUMO+1
T_1	2.1915	–	π-π*	HOMO → LUMO
T_2	2.8655	–	n-π*	HOMO–4 → LUMO

T_3	2.9294	–	n-π*, π-π*	HOMO–6 → LUMO, HOMO → LUMO+1
T_4	2.9458	–	π-π* (CT)	HOMO–1 → LUMO
T_5	3.0129	–	π-π* (CT)	HOMO–2 → LUMO
T_6	3.1624	–	π-π*	HOMO → LUMO+1
T_7	3.3572	–	π-π* (CT)	HOMO–3 → LUMO, HOMO–5 → LUMO
T_8	3.3654	–	π-π* (CT)	HOMO–5 → LUMO, HOMO–3 → LUMO

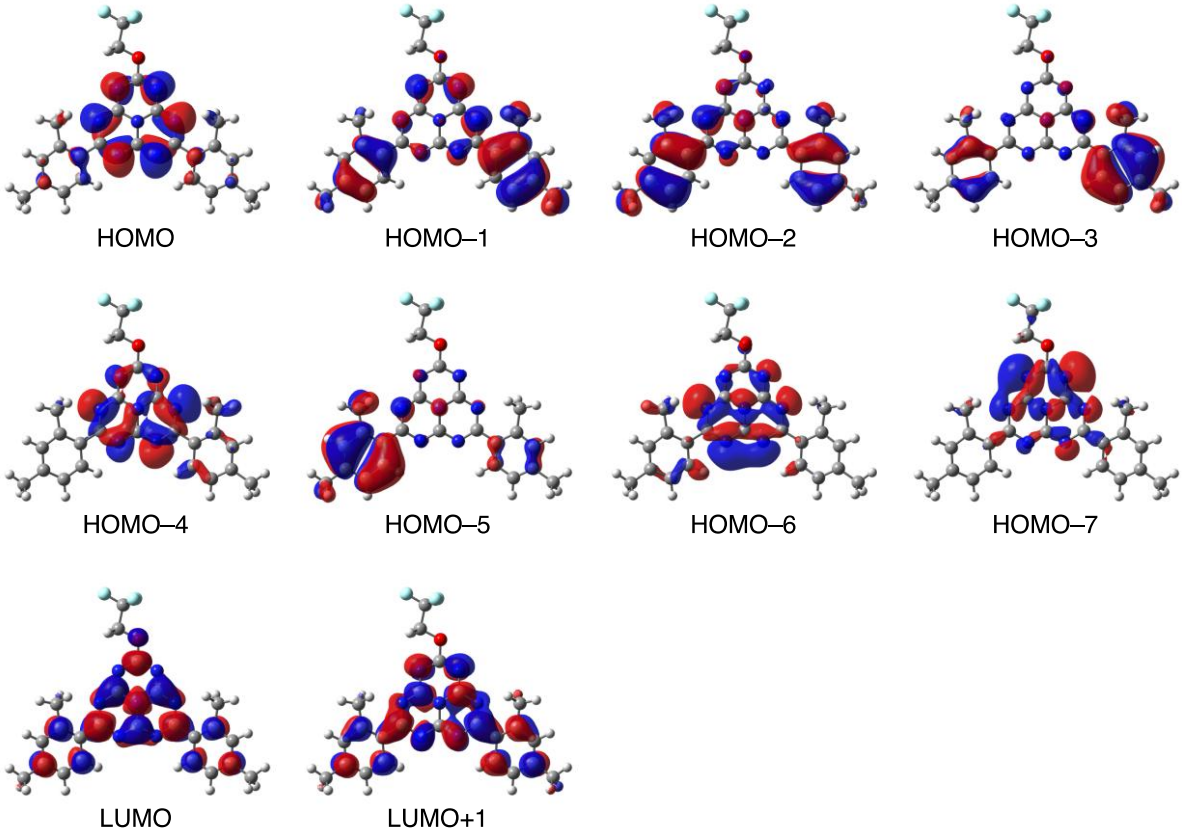

Fig S66. Theorical modelling of electronic transitions. Molecular orbitals at the S_1 optimized structure for $HzTFEX_2$.

8. Methods

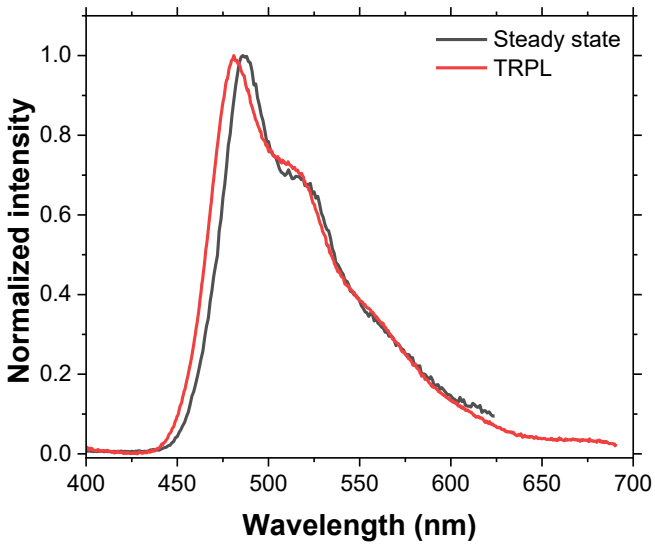

Fig S67. Correlation between steady state and time-resolved data. PL and TRPL of prompt emission of $HzTFEX_2$ in toluene 2 μM air saturated solution. λ_{ex} = 355 nm.

8. References

1. Krause, J. K. & Dodrill, B. C. Measurement system induced errors in diode thermometry. *Rev. Sci. Inst.* **57**, 661–665 (1986).

2. Sarkar, R. *et al.* An NMR thermometer for cryogenic magic-angle spinning NMR: The spin-lattice relaxation of 127I in cesium iodide. *J. Mag. Reson.* **212**, 460–463 (2011).

3. Scott, D. W. *et al.* Toluene: thermodynamic properties, molecular vibrations, and internal rotation. *J. Phys. Chem.* **66**, 911–914 (2002).